ELECTRONIC INSTRUMENTATION FOR ONLINE MONITORING OF DISSIPATION FACTOR

A dissertation submitted in partial fulfillment of the requirements

for the degree of

Master of Technology

by

Suhas P. Solanki

(*Roll No. 00307902*)

under the guidance of

Prof. P. C. Pandey

Prof. S. V. Kulkarni

Department of Electrical Engineering

Indian Institute of Technology, Bombay

Powai, Mumbai 400 076

January 2003

INDIAN INSTITUTE OF TECHNOLOGY, BOMBAY

DISSERTATION APPROVAL

Dissertation entitled: ELECTRONIC INSTRUMENTATION FOR ONLINE MONITORING OF DISSIPATION FACTOR

by **Suhas P. Solanki**

is approved for the award of the degree of MASTER OF TECHNOLOGY in Electrical Engineering.

Supervisors	______________________	(Prof. P. C. Pandey)
	______________________	(Prof. S. V. Kulkarni)
Internal Examiner	______________________	(Prof. T. S. Rathore)
External Examiner	______________________	(Dr. S. R. Kannan)
Chairperson	______________________	(Prof. D. N. Singh)

Date: 28^{th} January, 2003.

Acknowledgement

I would like to express my deepest gratitude to my guides Prof. P.C. Pandey and Prof. S.V. Kulkarni for their guidance, support, and encouragement throughout the course of this project. I would like to thank Prof. T.S. Rathore and Prof. T. Anjaneyulu for the kind support and suggestions I have received from them.

I am thankful to Mr. Dinesh Choudhary and Mr. Vidyadhar Kamble for their guidance in hardware circuitry and PCB fabrication, my lab colleagues Ashwin Athram and Parveen Lehana for their kind support, and Mr. Ritesh Parekh, Mr. Amol Sawant and their colleagues from M/s Crompton Greaves for the high voltage setup. I would also like to extend my sincere thanks to Mr. L.D. Muntode of our laboratory for his help and support during this project.

Suhas P. Solanki

January 2003

Suhas P. Solanki / Prof. P.C. Pandey and Prof. S.V. Kulkarni (supervisors): "Electronic instrumentation for online monitoring of dissipation factor", *M.Tech. dissertation*, Dept. of Electrical Engineering, Indian Institute of Technology, Bombay, January 2003.

Abstract

A technique for online monitoring of dissipation factor in the range of 5–50 $\times 10^{-3}$, with a precision better than 5×10^{-5} is investigated using numerical simulation and by using experimental set-up. The dissipation factor is obtained by processing the simultaneously sampled signals corresponding to voltage and current, and involves dividing the low-pass filtered product of voltage and current signals by the RMS values of the two signals. The measurement update rate depends on the response time of the low pass filters. It is shown that the desired precision can be obtained using (a) sampling rate much larger than the power line frequency, giving high update rate, (b) sampling rate lower than the power line frequency and processing the aliased periodic waveforms retaining the original phase relationship. The second method can be used for low cost instrumentation for condition monitoring applications with low measurement update rate. Both the methods need floating point arithmetic for processing.

Contents

List of symbols

Symbol	Explanation
γ	Normalized cut-off frequency (f_c / f_s)
δ	Loss angle
σ	Standard deviation
ω_o	Angular frequency
f	Frequency
f_c	Cut off frequency
f_o	Power line frequency
f_s	Sampling rate
I	Current
L	Number of ADC bits
n	Samples
t	Time
V	Voltage
V_{pp}	peak-to-peak voltage
V_{s}	Supply voltage
V_{sample}	Sampling signal

List of abbreviations

Symbol	Explanation
ADC	Analog-to-digital converter
BPF	Band pass filter
DFT	Discrete fourier transform
DSO	Digital storage oscilloscope
FIR	Finite impulse response
I/V	Current to Voltage
LPF	Low pass filter
PC	Personal computer
p.s.d	Power density spectrum
RMS	Root mean square
sa/s	Samples/second

List of figures

List of tables

Chapter 1

Introduction

1.1 Problem overview

A capacitor with a lossy dielectric can be represented by a capacitor C_p in parallel with a resistor R_p as shown in Fig. 1.1. For sinusoidal voltage $v(t)$ of frequency ω, capacitive current component $i_C(t)$, resistive current component $i_R(t)$, and the net current $i(t)$ are given as,

$$v(t) = V_m \cos \omega t \tag{1.1}$$

$$i_C(t) = (\omega C_p V_m)\cos(\omega t + \pi/2) \tag{1.2}$$

$$i_R(t) = (V_m/R_p)\cos \omega t \tag{1.3}$$

$$i(t) = \sqrt{\omega^2 C_p^2 + R_p^{-2}}\, V_m \cos(\omega t + \pi/2 - \delta) \tag{1.4}$$

$$V = V_m/\sqrt{2} \tag{1.5}$$

$$I_C = \omega C_p V \tag{1.6}$$

$$I_R = V/R_p \tag{1.7}$$

$$I = \sqrt{I_C^2 + I_R^2} \tag{1.8}$$

$$\tan\delta = I_R/I_C = (\omega C_p R_p)^{-1} \tag{1.9}$$

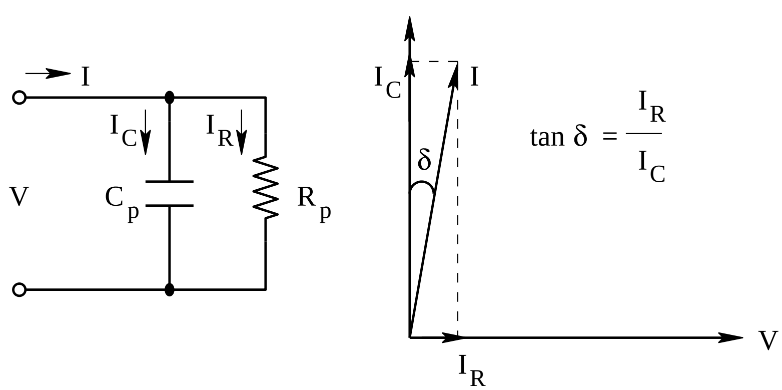

Fig. 1.1 Equivalent parallel RC circuit for a capacitor with lossy dielectric

The net current I lags the capacitive current component I_C by loss angle δ, and leads the resistive current component by angle $\pi/2 - \delta$.

The capacitor with the lossy dielectric may also be modeled as a capacitor C_s in series with resistor R_s as shown in Fig.1.2. Here,

$$\tan\delta = V_R/V_C = \omega C_s R_s \tag{1.10}$$

The net voltage V lags the voltage across the capacitor V_c by the loss angle δ, and leads the voltage across the resistor by angle $\pi/2 - \delta$.

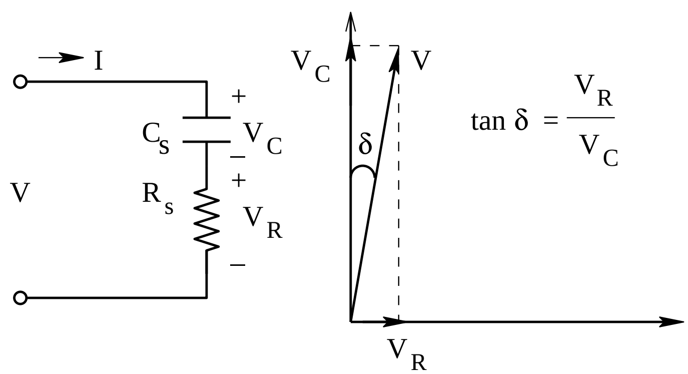

Fig. 1.2 Equivalent series RC circuit for a capacitor with lossy dielectric

The factor tanδ given by (1.9) in case of a parallel model or (1.10) in case of series model is known as dissipation factor [1],[2]. For small values of δ, tan$\delta \approx$ sin$\delta \approx \delta$.

When a dielectric is used for insulation in high voltage applications, the loss angle goes on increasing as the insulation condition deteriorates. The measurement of the loss angle or dissipation factor can serve as one of the several techniques for condition monitoring of insulation [3]. To ensure safe and reliable operation of high voltage equipment, it is necessary to monitor periodically the condition of insulation used in it. This can be accomplished by measuring the dielectric dissipation factor using conventional techniques such as Schering bridge [4]. These offline measurements require the removal of equipment from service, and hence cannot be carried out very frequently. Insulation deterioration during the interval between scheduled testing is typically undetected, introducing a significant risk element, particularly in the case of aging equipment. Further the offline testing is performed with equipment in switched off condition. When the equipment is in service, as the load increases the temperature also increases. It is well known that tanδ value increases with temperature. Hence reliability and accuracy of the measurements taken in offline mode are questionable as the operational conditions of the high voltage equipment cannot be fully duplicated [2]. This disadvantage can be overcome by using online measurements, because they offer the possibility of continuous monitoring of the insulation under operating conditions.

1.2 Review of techniques

Instrumentation for online monitoring of dissipation factor based on the Schering bridge technique has been reported [5][6], with a computer monitoring system replacing the conventional null detector. The application of this method to diagnose the state of current transformer insulation in a substation is discussed. The measured values of dielectric dissipation factor are compared with data from similar units at the substation operating under identical conditions and the trends are analyzed to get an indication of the condition/failure of insulation.

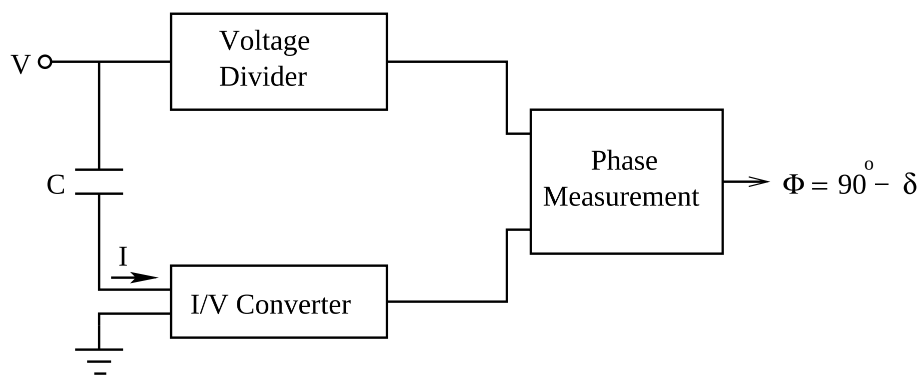

Fig. 1.3 Setup for phase measurement

Measurement of the phase angle between the voltage and the current signals can be used as a direct method for online monitoring of the loss angle and the dissipation factor, without requiring a reference set-up, and a number of investigations have been reported [7]-[13]. Fig. 1.3 shows the general schematic arrangement for measuring the loss angle of insulation under test in case of high voltage apparatus. The capacitor C under test is connected to high voltage level, and a voltage divider provides the voltage signal. The current through the capacitor is converted to voltage by I/V converter. The two output signals are given to the phase measuring circuit which gives Φ, and 90°-Φ is the loss angle δ. Measurement of the phase angle with a resolution appropriate for monitoring variation in δ, at power frequencies in the presence of harmonic distortion and noise, requires special considerations.

The conventional approach for phase measurement consists of converting the signals into square waveform by means of zero crossing detector and then measuring the time difference between the pulse edges [7] or centers of the square waveforms [8]. The time difference can be measured as a time interval either based on one period or averaged on a number of input signal periods [9]. In the presence of harmonics, these methods introduce errors or are unusable if signals have multiple zero crossings. Also the offsets and drifts in these zero crossing detectors can introduce severe errors.

The method based on detection of zero crossings is reported in [10]. The measured voltage and current signals are converted into rectangular waveforms and the phase difference is obtained by using logic gates and a high speed counter. The voltage and current signals are obtained using two caplinks (a parallel combination of R and C) with the same time constant. To obtain correct results, the values of the caplinks have to be chosen properly, so that the phase shift of applied voltage due to their insertion can be minimized. The measurement of relative tanδ between similar units minimizes harmonic influences.

The method proposed in [11] uses filtering of the current and voltage signals, and then zero crossing routine is used to find the dissipation factor. The voltage on the high voltage bus is sensed using an electro-optic electric-field sensor and the current is sensed by the drop across resistance connected as shunt. These signals are low pass filtered to remove noise and high pass filtered to remove DC. Once the data are filtered, the frequency is computed over 200 cycles long interval. The zero crossing routine is used to count the number of cycles and to find the exact position of the zero-crossings at the 0^{th} and 200^{th} cycle using interpolation. Using the sampling rate, number of cycles in the 200 cycles interval and portion of sample remaining between the 0^{th} and 200^{th} zero crossings, the frequency is calculated. The voltage signal is then shifted by a quarter cycle i.e. 90º. The number of samples in a quarter cycle is determined by using the frequency calculated, which need not be an integer. The tanδ value is expressed as a function of integer number of data samples taken in the 200 cycle long interval, portion of the sample remaining between the 0^{th} and 200^{th} zero crossings and the number of samples in a quarter cycle. The absolute value of dissipation factors are accurate to within ±0.005 based on comparisons with the measurements done using conventional bridge techniques.

The method proposed in [12] is based on the harmonic analysis using the DFT. The measurements were performed on a 230 kV current transformer unit. The analog voltage and current signals were scaled down and passed through signal conditioning unit, which provides low pass filtering and isolation of input analog signals. An 8-bit resolution digital storage oscilloscope was used to implement the simultaneous sampling of the analog voltage and current signals. The dissipation factor was obtained from the phase information of fundamental components by using DFT. The measurement precision of this method was ± 0.0005 for dielectric dissipation factor ranging from 0.001 to 0.02 for the sampling rate of 200 k sa/s.

A different method of high precision phase angle measurement between two periodic signals, based on digital filtering, used for extraction of the input signal fundamental harmonics, is presented in [13]. This technique does not require synchronous sampling; only constant sampling frequency is required. The technique provides frequency insensitive operation in frequency band as wide as ±10% around the nominal frequency. Its main field of application is in the measurements of distorted waveforms at power frequencies. In the filtering process, the transition band should be narrow and the attenuation in stop band should be very high to eliminate higher order harmonics. The deviations in the pass and stop band should cause less than ½ LSB variations in an *n*-bit ADC, so that the deviations are not detected. The paper describes the method of multi-rate filtering to overcome the constraints of filter design. It is found that there is a reduction in the filter order by a decade, but instead of a single filter, two filters are required. This method can resolve phase differences of 5 μ-radians with an uncertainty of less than 25 μ-radians.

1.3 Project objective

The dissipation factor can be monitored by continuously acquiring the voltage $v(t)$ applied across the capacitor and the current $i(t)$ passing through it and calculating the dissipation factor by dividing the low-pass filtered product of voltage and current signals by the RMS values of the two signals, i.e. by dividing the actual power by apparent power. An error analysis of this technique for studying the effect of number of quantization bits and other processing parameters has been carried out by the author's supervisor [14]. The objective of this project is to carry out a verification of the technique by numerical simulation and to develop a low cost electronic instrumentation for online monitoring of the dissipation factor. Towards this end, a low cost data acquisition card with 2-channel simultaneous 12-bit signal acquisition and serial interface is developed and aliasing of periodic waveforms is used to carry out the processing at a sampling rate lower than the power line frequency.

1.4 Report outline

The proposed method of online dissipation factor measurement along with theoretical error analysis is presented in Chapter 2. In Chapter 3, the technique of sampling at a high rate is discussed and the results of simulation are presented, along with those from an experimental setup. In Chapter 4, the technique of sampling the signal at a rate lower than the power line frequency is presented along with the results of simulation, and experimental hardware setup. Chapter 5 gives the summary and scope for future work.

Chapter 2

Proposed technique and error analysis

2.1 Basic technique

The technique is based on the principle of sampling the two input signals, corresponding to the voltage applied across the capacitor and the current passing through it, and carrying out digital processing of these signals for calculating the dissipation factor, basically by taking the ratio of actual power to apparent power. The block diagram of the technique is shown in Fig. 2.1.

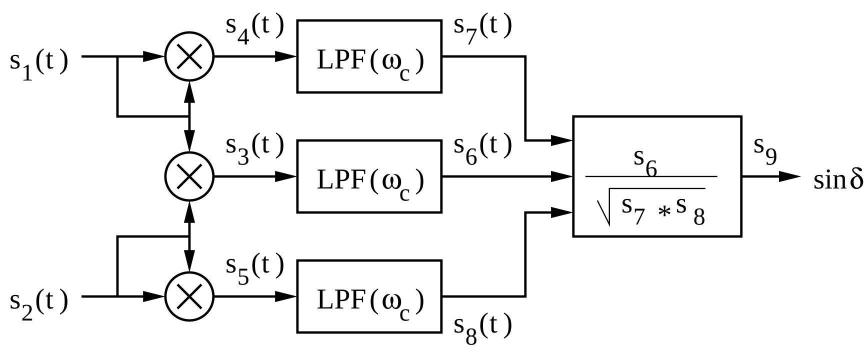

Fig.2.1 Block diagram of technique used for dissipation factor measurement [14]

The two input signals $s_1(t)$ and $s_2(t)$, correspond to voltage and current respectively.

$$s_1(t) = A \cos(\omega_o t) \tag{2.1}$$

$$s_2(t) = B \cos(\omega_o t + 0.5\pi - \delta) \tag{2.2}$$

where ω_o is the power line frequency and δ is the loss angle. The product of these two waveforms is,

$$s_3(t) = s_1(t)\, s_2(t) = 0.5AB\left[\cos(2\omega_o t + 0.5\pi - \delta) + \sin\delta\right] \tag{2.3}$$

The squares of the two input waveforms are,

$$s_4(t) = [s_1(t)]^2 = 0.5A^2 \left[1 + \cos(2\omega_o t)\right] \tag{2.4}$$

$$s_5(t) = [s_2(t)]^2 = 0.5B^2 \left[1 + \cos\ 2(\omega_o t + 0.5\pi - \delta)\right] \tag{2.5}$$

These waveforms are low pass filtered with cut off frequency $\omega_c << \omega_o$ to retain only the dc components, and we get

$$s_6(t) = \text{LPF}\{s_3(t)\} = 0.5AB\sin\delta \tag{2.6}$$

$$s_7(t) = \text{LPF}\{s_4(t)\} = 0.5A^2 \tag{2.7}$$

$$s_8(t) = \text{LPF}\{s_5(t)\} = 0.5B^2 \tag{2.8}$$

From these equations, we obtain

$$s_9 = s_6 \big/ \sqrt{s_7 s_8} = \sin\delta \tag{2.9}$$

And the dissipation factor is given as,

$$\tan\delta = \tan\left[\sin^{-1} s_9\right] \tag{2.10}$$

Since the value of δ is generally very small, $\cos\delta \approx 1$, hence $\tan\delta \approx \delta \approx \sin\delta = s_9$

2.2 Error analysis [14]

Error in the estimation of δ will depend on the number of quantization bits, sampling rate used and filter parameters. The effect of quantization may be modeled as additive random noise [15][16]. Each quantized and sampled waveform $x(n)$ is the sum of the true signal waveform $s(n)$ and quantization noise $e(n)$. Thus we have,

$$x_1(n) = s_1(n) + e_1(n) \tag{2.11}$$

$$x_2(n) = s_2(n) + e_2(n) \tag{2.12}$$

These result in,

$$x_3(n) = x_1(n)x_2(n) = s_1 s_2 + s_1 e_2 + s_2 e_1 + e_1 e_2 \tag{2.13}$$

$$x_4(n) = [x_1(n)]^2 = s_1^2 + e_1^2 + 2s_1 e_1 \tag{2.14}$$

$$x_5(n) = [x_2(n)]^2 = s_2^2 + e_2^2 + 2s_2 e_2 \tag{2.15}$$

After low pass filtering these waveforms, we get

$$\begin{aligned} x_6(n) &= \text{LPF}\{x_3(n)\} = \text{LPF}\{s_1 s_2\} + \text{LPF}\{s_1 e_2 + s_2 e_1 + e_1 e_2\} \\ &= s_6 + e_6 \end{aligned} \tag{2.16}$$

$$\begin{aligned} x_7(n) &= \text{LPF}\{x_4(n)\} = \text{LPF}\{s_1^2\} + \text{LPF}\{e_1^2 + 2s_1 e_1\} \\ &= s_7 + e_7 \end{aligned} \tag{2.17}$$

$$x_8(n) = \mathrm{LPF}\{x_5(n)\} = \mathrm{LPF}\{s_2^2\} + \mathrm{LPF}\{e_2^2 + 2s_2e_2\}$$
$$= s_8 + e_8 \tag{2.18}$$

where s_6, s_7, s_8 are the same as before. Terms e_6, e_7, e_8 have resulted due to quantization noise, i.e. we are assuming that the second order harmonic terms have been eliminated by low pass filtering, but a finite amount of broad band quantization noise has remained due to the finite bandwidth of the low pass filter.

Now from x_6, x_7 and x_8 we get ,

$$x_9 = \frac{x_6}{\sqrt{(x_7x_8)}} = \frac{0.5AB\sin\delta + e_6}{\sqrt{(0.5A^2 + e_7)}\sqrt{(0.5B^2 + e_8)}}$$
$$= \frac{\sin\delta + 2e_6/AB}{\sqrt{(1+2e_7/A^2)}\sqrt{(1+2e_8/B^2)}} \tag{2.19}$$

Assuming the quantization noise magnitudes to be very small compared to the values of *A* and *B*, we get

$$x_9 \approx \left(\sin\delta + \frac{2e_6}{AB}\right)\left(1 - \frac{e_7}{A^2}\right)\left(1 - \frac{e_8}{B^2}\right)$$
$$\approx \left(\sin\delta + \frac{2e_6}{AB}\right)\left(1 - \frac{e_7}{A^2} - \frac{e_8}{B^2}\right)$$

Further, ignoring the second order error terms, we get

$$x_9 \approx \sin\delta + \frac{2e_6}{AB} - \sin\delta\left(\frac{e_7}{A^2} + \frac{e_8}{B^2}\right)$$
$$= \sin\delta + e_9 \tag{2.20}$$

The error term in the final result can be written as,

$$e_9 = (2/AB)\,e_6 - \sin\delta\left(e_7/A^2 + e_8/B^2\right)$$
$$= 2\,\mathrm{LPF}\{(e_1s_2 + e_2s_1 + e_1e_2)/AB\} - \sin\delta\,\mathrm{LPF}\{(e_1^2 + 2e_1s_1)/A^2 + (e_2^2 + 2e_2s_2)/B^2\}$$

Ignoring the second order errors, and combining together the error terms involving e_1 and e_2, we get

$$e_9 = 2\,\mathrm{LPF}\{e_1(s_2/AB - s_1\sin\delta/A^2) + e_2(s_1/AB - s_2\sin\delta/B^2)\}$$
$$= 2\,\mathrm{LPF}\{(e_1/A)(\cos(2\pi f_o n/f_s + \pi/2 - \delta) - \sin\delta\cos(2\pi f_o n/f_s))$$
$$+ (e_2/B)(\cos(2\pi f_o n/f_s) - \sin\delta\cos(2\pi f_o n/f_s + \pi/2 - \delta))\}$$

$$= 2\,\mathrm{LPF}\{(e_1/A)(-\cos\delta\sin(2\pi f_o n/f_s)) + (e_2/B)(\cos\delta\cos(2\pi f_o n/f_s - \delta))\}$$

$$= 2\cos\delta[-(1/A)\mathrm{LPF}\{e_1\sin(2\pi f_o n/f_s)\} + (1/B)\mathrm{LPF}\{e_2\cos(2\pi f_o n/f_s - \delta)\}]$$

We can write the above as,

$$e_9 = 2\cos\delta[-r_1/A + r_2/B] \tag{2.21}$$

where

$$r_1 = \mathrm{LPF}\,\{e_1\sin(2\pi f_o n/f_s)\}$$

$$r_2 = \mathrm{LPF}\,\{e_2\cos(2\pi f_o n/f_s - \delta)\}$$

It is to be noted that r_1 and r_2 are random noises associated with the process of quantization of signals s_1 and s_2 respectively, and hence they are uncorrelated with each other. Therefore, the mean squared value of the error e_9 is given as,

$$\sigma_{e9}^2 = 4\cos^2\delta\left[\sigma_{r1}^2/A^2 + \sigma_{r2}^2/B^2\right] \tag{2.22}$$

For sampling rate of f_s and quantization step of Δ, the quantization error [15] [16] can be modeled as random noise with uniform power spectrum density over [$-f_s/2$, $f_s/2$] with ac RMS value given as,

$$\sigma_e = \Delta/\sqrt{12} \tag{2.23}$$

In order to estimate the RMS value of the error, we need to obtain estimate of random white noise waveform modulated by a sinusoid and low pass filtered. Let us consider a waveform $p(n)$ generated by multiplying random white noise $e(n)$ having ac RMS value of σ_e with a sinusoidal waveform of frequency f_o ($<f_s/2$),

$$p(n) = e(n)\cos(2\pi f_o n/f_s + \theta) \tag{2.24}$$

Its autocorrelation is,

$$R_p(n) = (1/2)R_e(n)\cos(2\pi f_o n/f_s)$$

and therefore, the power spectrum density (p.s.d) of $p(n)$ is

$$S_p(f) = (1/4)[S_e(f - f_s) + S_e(f + f_s)]$$

where $S_e(f)$ is the p.s.d. of $e(n)$. Considering $e(n)$ as noise with uniform p.s.d. S_e over [$-f_s/2$, $f_s/2$] and RMS value of σ_e, we have

$$S_e = \sigma_e^2/f_s$$

Since $f_s/2 > f_o$, we get the p.s.d of $p(n)$ as

$$S_p(f) = S_e/2\text{, for } |f| < f_s/2 - f_o$$

$$S_e/4\text{, for } f_s/2 - f_o < |f| < f_s/2 + f_o$$

$$0\text{, for } |f| > f_s/2 + f_o$$

Signal $q(n)$ is the output of the low pass filter $H(f)$. Therefore, the p.s.d. of $q(n)$ is

$$S_q(f) = |H(f)|^2 S_p(f)$$

If the filter has a cut off frequency $f_c < f_s/2 - f_o$, then

$$S_q(f) = S_e/2\text{, for } |f| < f_c$$

$$0\text{, for } |f| > f_c$$

therefore the mean square value of $q(n)$ is given by

$$\sigma_q^2 = (S_e/2)(2f_c) = \sigma_e^2(f_c/f_s)$$

Therefore,

$$\sigma_q = \sigma_e\sqrt{f_c/f_s} \tag{2.25}$$

Using this result, the mean squared value of error e_9 as given in (2.21) may be given as

$$\sigma_{e9}^2 = 4\cos^2\delta(f_c/f_s)(\sigma_{e1}^2/A^2 + \sigma_{e2}^2/B^2) \tag{2.26}$$

For signal range of ($-V_m$, $+V_m$) and L-bit uniform quantization, the quantization step is,

$$\Delta = 2V_m/2^L \tag{2.27}$$

and therefore, the ac root mean squared values of the quantization errors in the two inputs are

$$\sigma_{e1} = \sigma_{e2} = \sigma_e = \frac{2V_m}{2^L\sqrt{12}} \tag{2.28}$$

Let the peak value of the two input signals be,

$$A = \alpha_1 V_m$$

$$B = \alpha_2 V_m$$

Then, $$\sigma_{e9} = (2\cos\delta)\left(\frac{1}{2^L}\right)\left(\frac{1}{\sqrt{3}}\right)\sqrt{\left(\frac{1}{\alpha_1^2} + \frac{1}{\alpha_2^2}\right)}\sqrt{\frac{f_c}{f_s}} \tag{2.29}$$

For the special case of $\alpha_1 = \alpha_2 = 1$ (i.e., both the input signals occupy the full range of the ADC's), we get

$$\sigma_{e9} = \sqrt{\frac{8}{3}} \cos\delta \left(\frac{1}{2^L}\right) \sqrt{\frac{f_c}{f_s}}$$

For small values of δ, $\cos\delta \approx 1$ and therefore

$$\sigma_{e9} = \left(\frac{1}{2^L}\right) \sqrt{\frac{8 f_c}{3 f_s}} \tag{2.30}$$

If we define the normalized cutoff frequency of digital low pass filter as

$$\gamma = f_c / f_s \tag{2.31}$$

then the ac RMS value of the error can be written as

$$\sigma_{e9} = 2^{-L} \sqrt{8\gamma/3} \tag{2.32}$$

The values of σ_{e9} as given by (2.32) are calculated and given in Table 2.1 for some specific values of L and $\gamma = f_c / f_s$. Table 2.2 gives the value of γ for some specific values of L and σ_{e9}.

For condition monitoring of insulation in transformers, dissipation factor of interest is generally in the range 0.005 – 0.05. For 1 % resolution at the low end of the range, we should have $\sigma_e < 5\times10^{-5}$. To achieve this with L = 8 and 12, we require γ = 6.14×10^{-5} and 1.57×10^{-2} respectively, for f_o = 50 Hz and f_s = 50 k sa/s, this will require f_c = 3 Hz and 786 Hz respectively.

Table 2.1 Theoretical estimates of RMS values of error, σ_{e9}, caused by input quantization. L = number of quantization bits, $\gamma = f_c / f_s$.

L	**σ_{e9}**					
	γ = 0.5	**γ = 0.1**	**γ = 0.01**	**γ =10^{-3}**	**γ = 10^{-4}**	**γ = 10^{-5}**
1	0.58	0.26	0.82e-01	0.26e-01	0.82e-02	0.26e-02
4	0.72e-01	0.32e-01	0.1e-01	0.32e-02	0.1e-02	0.32e-03
8	0.45e-02	0.20e-02	0.64e-03	0.2e-03	0.64e-04	0.2e-04
12	0.28e-03	0.13e-03	0.40e-04	0.13e-04	0.40e-05	0.13e-05
16	0.18e-04	0.79e-05	0.25e-05	0.79e-06	0.25e-06	0.79e-07

Table 2.2 Theoretical estimates of the low pass normalized cut-off frequency γ (= f_c / f_s), for specific values of L and RMS values of error σ_{e9}.

L	**γ**						
	σ_{e9}=10^{-3}	σ_{e9}=5×10^{-4}	σ_{e9}=10^{-4}	σ_{e9}=5×10^{-5}	σ_{e9}=10^{-5}	σ_{e9}=5×10^{-6}	σ_{e9}=10^{-6}
1	1.50e-06	3.75e-07	1.50e-08	3.75e-09	1.50e-10	3.75e-11	1.50e-12
4	9.60e-05	2.40e-05	9.60e-07	2.40e-07	9.60e-09	2.40e-10	9.60e-11
8	2.50e-02	6.14e-03	2.50e-04	6.14e-05	2.50e-06	6.14e-07	2.50e-08
12	6.30e-00	1.57e-00	6.30e-02	1.57e-02	6.29e-04	1.57e-04	6.29e-06

Chapter 3

Implementation with high sampling rate

The technique presented in the previous chapter was verified by numerical simulation with a high sampling rate, for finding out the errors in the measurement. Subsequently, an experimental setup was used to understand some of the practical problems in implementation. Signal acquisition was done using a digital storage oscilloscope and processing was done using a PC. Two setups were used, first a low voltage setup and then a high voltage setup. The results obtained are presented.

3.1 Numerical simulation

To calculate the dissipation factor of the dielectric, we need the voltage applied across the capacitor and the current through it. Let

$$s_1(n) = V_m \cos(2\pi\, n\, f_o / f_s) \tag{3.1}$$

$$s_2(n) = I_m \cos(2\pi n\, f_o / f_s + 0.5\pi - \delta) \tag{3.2}$$

where f_o is the power line frequency, f_s is the sampling rate, δ is the loss angle and n is the sample index. Numerical simulation was carried out with V_m=1, I_m =1, f_o = 50 Hz, and f_s = 50 k sa/s, for loss angle in the range of 0.005 to 0.05.

The waveform synthesis and the entire processing was done using floating point representation, in order to avoid recursion and saturation errors related to fixed point representation in digital processing [15]. For simulating the effect of L-bit quantization, the waveform was multiplied by 2^{L-1} and rounded to the nearest integer. The rounded off integer was divided by 2^{L-1} to get the quantized sequence. Sequences $x_3 = x_1^2$, $x_4 = x_2^2$, and $x_5 = x_1 x_2$ were low pass filtered to get x_6, x_7, x_8. Dissipation factor was calculated as $x_9 = x_6 \big/ \sqrt{x_7 x_8}$.

Investigations were carried out for different values of L and several types of filter for processing. In the following description these are referred to as simulations A, B, C, D, and E.

In simulation A, the low pass filter used was a FIR filter, designed using rectangular window [17]. The processing results, after the stabilization of the filter output were used for tabulation. Table 3.1 shows the simulation results for mean, maximum, minimum and standard deviation of s_9 for f_o = 50 Hz, f_s = 50 k sa/s, 10 k length low pass FIR filter (with $f_c \approx 5$ Hz), and $L = 16$ bits. The results were obtained for total sample length of 50 k and the results are based on the last 40 k samples. For δ : 0 – 0.05, we see that the mean values have excellent match. The standard deviation is less than 0.5×10^{-6}. For comparison, the theoretical error estimate, as given in Table 2.1, is $\sigma = 0.25 \times 10^{-6}$ for $L = 16$, $\gamma = 10^{-4}$.

Table 3.1 Results of numerical simulation A: f = 50 Hz, f_s = 50 k sa/s, L = 16 bits. LPF: 10 k order FIR (using rectangular window) with $f_c \approx 5$ Hz or $\gamma = 10^{-4}$.

δ (radians)	s_9 mean	s_9 max	s_9 min	σ
0	1.32211e-07	3.34794e-05	6.29851e-08	1.27302e-07
0.005	5.00973e-03	5.01056e-03	5.00923e-03	4.95241e-07
0.006	5.99205e-03	5.99211e-03	5.99200e-03	2.86675e-07
0.007	6.99289e-03	6.99296e-03	6.99284e-03	2.52522e-07
0.008	7.99012e-03	7.99015e-03	7.99008e-03	2.15398e-07
0.009	8.99571e-03	8.99574e-03	8.99566e-03	2.06571e-07
0.01	9.96208e-03	9.96235e-03	9.96168e-03	1.69266e-07
0.02	1.99907e-02	1.99910e-02	1.99899e-02	2.41229e-07
0.03	2.99897e-02	2.99903e-02	2.99891e-02	3.92836e-07
0.04	3.99777e-02	3.99781e-02	3.99772e-02	1.60960e-07
0.05	4.99362e-02	4.99366e-02	4.99358e-02	2.57752e-07

It may be assumed that band pass filtering the two waveform before calculation of s_9, will reduce the input quantization error and may result in overall error reduction. For simulation B, the two waveforms x_1 and x_2 were pre-processed by band pass filtering with pass-band of 49 – 51 Hz. The band pass filter used was a FIR filter of order 1000 designed using a Hamming window [17]. We see from Table 3.1, that the standard deviation is unrelated to the value of δ and is less than 0.5×10^{-6}. Comparing the results in Table 3.2 with those in Table 3.1, we infer that for the synthesized waveform, band pass filtering does not give a large improvement in standard deviation in this case.

Table 3.2 Results of numerical simulation B: f_o = 50 Hz, f_s = 50 k sa/s, L = 16 bits. BPF: 1000 order FIR (using Hamming window) with pass band range of 49–51 Hz. LPF: 10 k order FIR (using rectangular window) with $f_c \approx 5$ Hz or $\gamma = 10^{-4}$.

δ (radians)	s_9 mean	s_9 max	s_9 min	σ
0	1.55495e-07	3.72530e-07	-4.16504e-08	6.09315e-08
0.005	5.00025e-03	5.00086e-03	4.99983e-03	2.67558e-07
0.006	5.98834e-03	5.98867e-03	5.98804e-03	1.20821e-07
0.007	7.00667e-03	7.00698e-03	7.00635e-03	1.18322e-07
0.008	7.96788e-03	7.96872e-03	7.96728e-03	3.76551e-07
0.009	9.03343e-03	9.03392e-03	9.03297e-03	2.45249e-07
0.01	9.99505e-03	9.99548e-03	9.99463e-03	1.84794e-07
0.02	2.00170e-02	2.00174e-02	2.00166e-02	1.28664e-07
0.03	2.99940e-02	2.99945e-02	2.99937e-02	1.77363e-07
0.04	3.99842e-02	3.99846e-02	3.99837e-02	2.69191e-07
0.05	4.99676e-02	4.99681e-02	4.99673e-02	2.59472e-07

Next, the simulations were carried out at different input frequencies in 49–51 Hz range. As the power line frequency was changed, a large variation in the standard deviation was observed. For f_o = 49.8 Hz in Table 3.3, we see that the standard deviation is of the order of 10^{-3}. It is to be noted that the FIR filter response has notches at multiples of 5 Hz and hence the second harmonic products are greatly attenuated for f_c = 50 Hz. This does not happen for 49.8 Hz and many other frequency values. Thus the large standard deviation is primarily contributed by the second harmonic and not by the broad band quantization noise. Hence we can try two solutions. The sampling rate can be selected to be an exact multiple of power line to ensure that the second harmonic is greatly attenuated. The second solution is to have an IIR filter that does not have any ripple in the stop band, so that a small drift in the power line frequency does not affect the standard deviation.

Simulation D was carried out using IIR filter of Butterworth type [17]. This kept the standard deviation low independent of the signal frequency variation over 49–51Hz. One of the results with Butterworth filter is shown in Table 3.4, for power line frequency f_o = 49.8 Hz, sampling frequency f_s = 50 k sa/s., and 4th order Butterworth type low pass filter with cut-off frequency f_c = 5 Hz. For δ : 0 – 0.05, standard deviation < 0.3×10^{-6}. Hence we conclude that IIR filter is the better option. Fig. 3.1 shows a plot of s_9 mean vs. tanδ for the results obtained in Table 3.4

Simulation E was carried out using the same Butterworth filter but with L = 8. The results of this simulation are given in Table 3.5. For δ : 0 – 0.05, standard deviation is less than 5×10^{-5}, which matches with theoretical estimate of 6.4×10^{-5} in Table 2.1. Fig. 3.2 shows a plot of s_9 mean vs. tanδ for the results obtained in Table 3.5

Table 3.3 Results of numerical simulation C: f_o = 49.8 Hz, f_s = 50 k sa/s, L = 16 bits. LPF: 10 k order (using rectangular window) with $f_c \approx$ 5 Hz or $\gamma = 10^{-4}$.

δ (radians)	s_9 mean	s_9 max	s_9 min	σ
0	1.27282e-05	3.97429e-03	-3.97429e-03	2.80795e-03
0.005	5.72996e-03	9.69129e-03	1.74298e-03	2.80795e-03
0.006	6.72399e-03	1.06856e-02	2.73698e-03	2.80796e-03
0.007	7.72594e-03	1.16873e-02	3.73891e-03	2.80795e-03
0.008	8.72510e-03	1.26865e-02	4.73817e-03	2.80795e-03
0.009	9.72376e-03	1.36854e-02	5.73677e-03	2.80795e-03
0.01	1.07227e-02	1.46841e-02	6.73587e-03	2.80795e-03
0.02	2.07227e-02	2.46842e-02	1.67356e-02	2.80795e-03
0.03	3.07174e-02	3.46787e-02	2.67304e-02	2.80795e-03
0.04	4.07135e-02	4.46751e-02	3.67265e-02	2.80795e-03
0.05	5.07068e-02	5.46682e-02	4.67198e-02	2.80795e-03

Table 3.4 Results of numerical simulation D: f_o = 49.8 Hz, f_s = 50 k sa/s, L = 16 bits. LPF: fourth order Butterworth with $f_c \approx$ 5 Hz or $\gamma = 10^{-4}$.

δ (radian)	s_9 mean	s_9 max	s_9 min	σ
0	-3.78555e-06	-3.45745e-06	-4.39289e-06	2.04947e-07
0.005	4.99300e-03	4.99334e-03	4.99232e-03	2.38295e-07
0.006	5.99097e-03	5.99134e-03	5.99028e-03	2.48625e-07
0.007	6.99168e-03	6.99204e-03	6.99109e-03	2.20424e-07
0.008	7.99117e-03	7.99154e-03	7.99059e-03	2.20379e-07
0.009	8.99191e-03	8.99220e-03	8.99128e-03	2.16406e-07
0.01	9.99057e-03	9.99087e-03	9.98991e-03	2.145911e-07
0.02	1.99909e-02	1.99911e-02	1.99900e-02	2.92417e-07
0.03	2.99838e-02	2.99843e-02	2.99831e-02	2.64700e-07
0.04	3.99828e-02	3.99831e-02	3.99821e-02	2.49205e-07
0.05	4.99788e-02	4.99790e-02	4.99782e-02	2.05446e-07

Table 3.5 Results of numerical simulation E : f_o = 50 Hz, f_s = 50 k sa/s, L = 8 bits. LPF: 4^{th} order Butterworth with $f_c \approx$ 5 Hz or $\gamma = 1.11\times10^{-4}$.

δ (radians)	s_9 mean	s_9 max	s_9 min	σ
0	3.71833e-06	2.23333e-04	-7.59154e-04	4.53539e-05
0.005	4.87297e-03	5.09081e-03	4.79412e-03	4.54180e-05
0.006	6.13823e-03	6.35618e-03	6.05938e-03	4.54344e-05
0.007	6.97834e-03	7.19563e-03	6.89927e-03	4.53222e-05
0.008	8.10254e-03	8.31763e-03	8.02414e-03	4.49198e-05
0.009	9.08412e-03	9.30178e-03	9.00514e-03	4.54260e-05
0.01	9.96917e-03	1.01871e-02	9.89042e-03	4.53987e-05
0.02	2.01501e-02	2.03669e-02	2.00700e-02	4.55199e-05
0.03	2.99705e-02	3.01882e-02	2.98904e-02	4.58314e-05
0.04	4.00673e-02	4.02899e-02	3.99946e-02	4.61868e-05
0.05	5.01086e-02	5.03237e-02	5.00267e-02	4.55190e-05

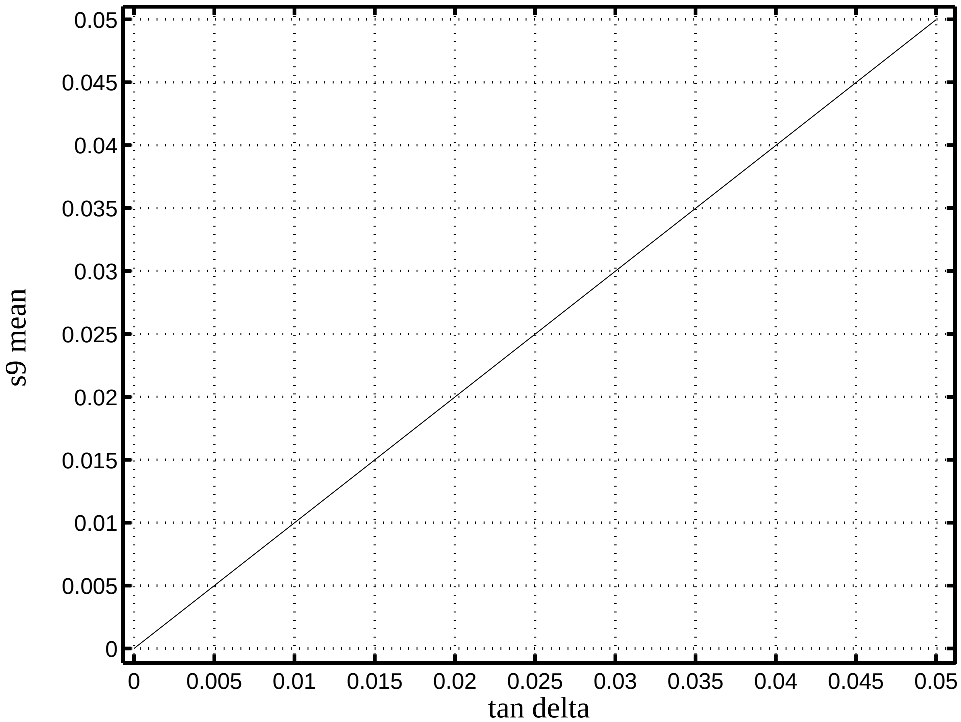

Fig. 3.1 Plot of s_9 mean vs. $\tan\delta$ for the results obtained in Table 3.4

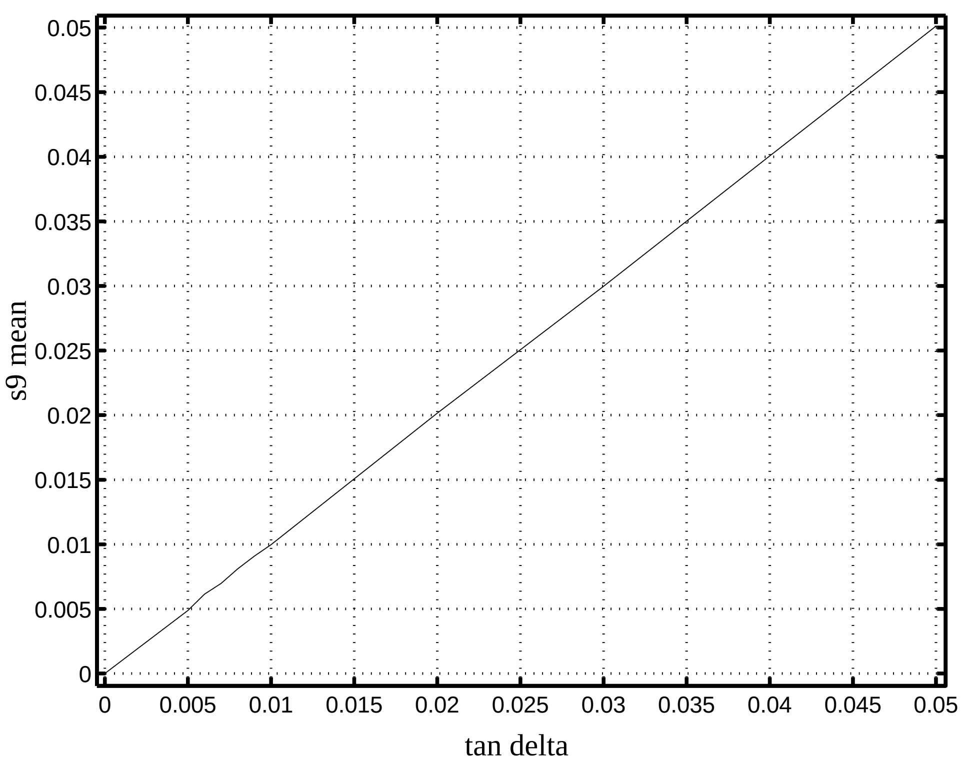

Fig. 3.2 Plot of s_9 mean vs. $\tan\delta$ for the results obtained in Table 3.5

3.2 Low voltage experimental setup

The circuit setup is shown in Fig. 3.3. Capacitor with lossy dielectric is formed by connecting ceramic capacitor C_x in series with resistor R_x. A range of tanδ values are obtained by changing R_x. Current through the capacitor is sensed by I-V converter circuit formed by op-amp U1 and resistors R_y and R_z. The excitation voltage is 30 V_{pp}, 50 Hz signal from a signal generator (Aplab 2019).

The voltage signal is obtained through a voltage divider consisting of resistors R_1 and R_2. Signal acquisition was done using a 2-channel, 8-bit simultaneous sampling DSO (Tektronix TDS-210). This instrument can record a maximum length of 2500 samples, and the record can be transferred using RS-232 interface and “Hyper terminal” software to a PC. The sample values obtained were formatted, scaled and processed.

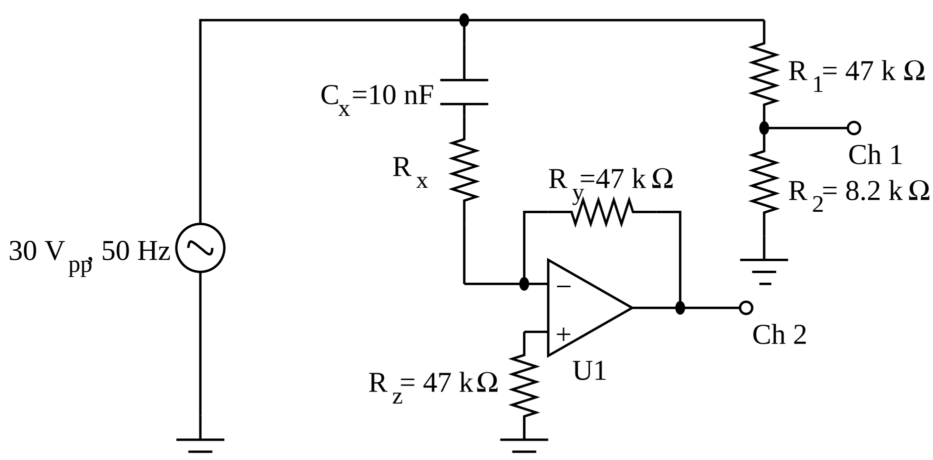

Fig. 3.3 Test setup using an I/V converter.

Due to the record length limit, a sample rate of 5 k sa/s. was used, giving record length of 0.5 s. Low pass filter used was a 1000-tap FIR filter designed using rectangular window. This filter has a cut off frequency of 5 Hz, i.e. $\gamma = 10^{-3}$. Table 3.6 gives the results. A plot of dissipation factor measured values versus test values (calculated from R_x and C_x) is shown in Fig.3.4. Best fit line, using GNUPLOT has a slope of 1.045 and offset of 1.662×10^{-4}, for median values. For average values, the slope and offset are 1.044 and 1.863×10^{-4} respectively.

Table 3.6 Results obtained using the setup of Fig.3.3. $L = 8$, $f_o = 50$ Hz, $f_s = 50$ k sa/s, $\gamma = 10^{-3}$, LPF: 1000-tap FIR. Measured $C_x = 10.43$ nF. R_x values are measured values.

R_X (Ω)	$\tan\delta = \omega C_x R_x$	s_9 average	s_9 median
266	8.715e-04	7.022e-04	6.927e-04
680	2.237e-03	2.243e-03	2.198e-03
1.018k	3.335e-03	3.942e-03	3.947e-03
1.493k	4.892e-03	5.416e-03	5.414e-03
2.19k	7.176e-03	7.803e-03	7.773e-03
2.67k	8.748e-03	9.432e-03	9.416e-03
3.27k	1.071e-02	1.161e-02	1.160e-02
3.86k	1.264e-02	1.345e-02	1.345e-02
4.67k	1.530e-02	1.656e-02	1.657e-02
5.55k	1.818e-02	1.852e-02	1.852e-02

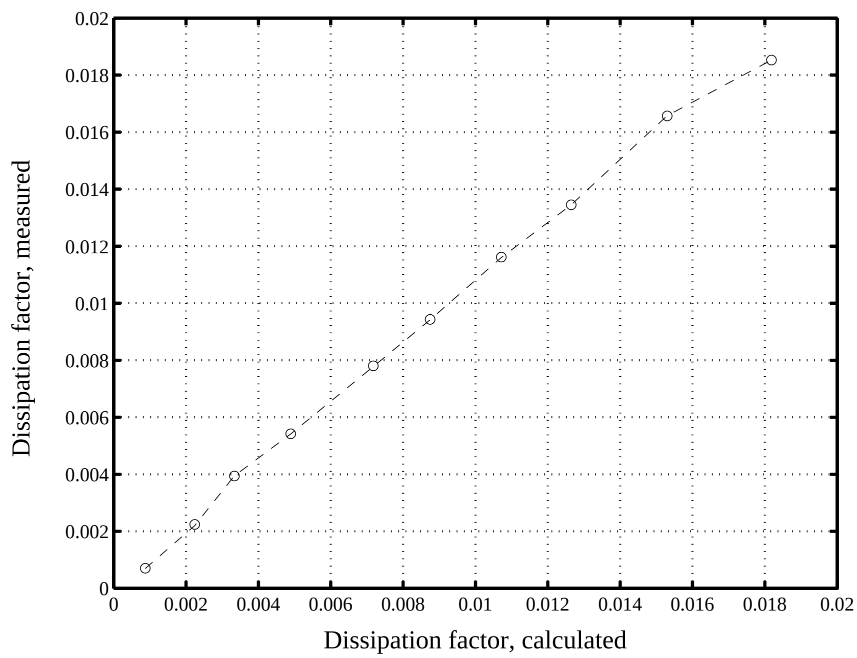

Fig. 3.4 Plot of dissipation factor measured values vs. calculated values for the circuit setup in Fig. 3.3.

3.3 High voltage experimental setup

The experiment was performed on the high voltage setup at the R&D division of M/s Crompton Greaves, Kanjurmarg, Mumbai. The supply source was derived from an auto-transformer setup. The readings were taken at 600 V rms and frequency of 50 Hz. The capacitance used was a standard air capacitor of 1000 pF which has four different series resistances and known set of tanδ values. The circuit of voltage front-end is given in Fig. 3.5. It uses a capacitive divider which has a gas filled capacitor of 98 pF with negligible losses and a low loss 0.2 μF polypropylene capacitor. A shunt resistance of 470 Ω is connected in the current front-end circuit as shown in Fig. 3.6. Resistor R_6 is used for input current limiting, and R_8 and R_4 are used for offset-null adjustment. Capacitors in the supply line C_{10}, C_{11}, C_{14} and C_{15} are dc bypass capacitors. With resistors R_2 and R_1, op-amp U1 acts as a non-inverting amplifier, with gain of $(1 + R_2/R_1)$. The signals were recorded using simultaneous sampling DSO (LeCroy 9304) at the rate of 50 k sa/s. with 8-bit resolution for record lengths of 50 k samples. The data for four different values of series resistances were stored in a floppy disk for both the current and voltage channels. The data were then transferred to a PC, formatted, scaled, and then processed using a FIR filter of order 10 k designed using rectangular window to obtain the average tanδ value. The cut-off frequency of this filter is 5 Hz, i.e. $\gamma = 10^{-4}$. The dissipation factor with shunt resistor R_{sh} is given by, $\tan\delta = \omega C_x (R + R_{sh})$.

Measurement results are given in Table 3.7. The plot of tanδ measured values vs calculated values (calculated from R, R_{sh}, C_x) is shown in Fig. 3.7. The best fit line using GNUPLOT has a slope of 1.051 and an offset of 5.7×10^{-4}.

Table 3.7 Dissipation factor for different values of resistance in series with standard capacitor for high voltage setup.

R (Ω)	**tanδ**	**s_9 average**
2850	1.147e-03	1.772e-03
1410	6.496e-04	1.262e-03
287	2.609e-04	8.400e-04
135	2.097e-04	7.049e-04

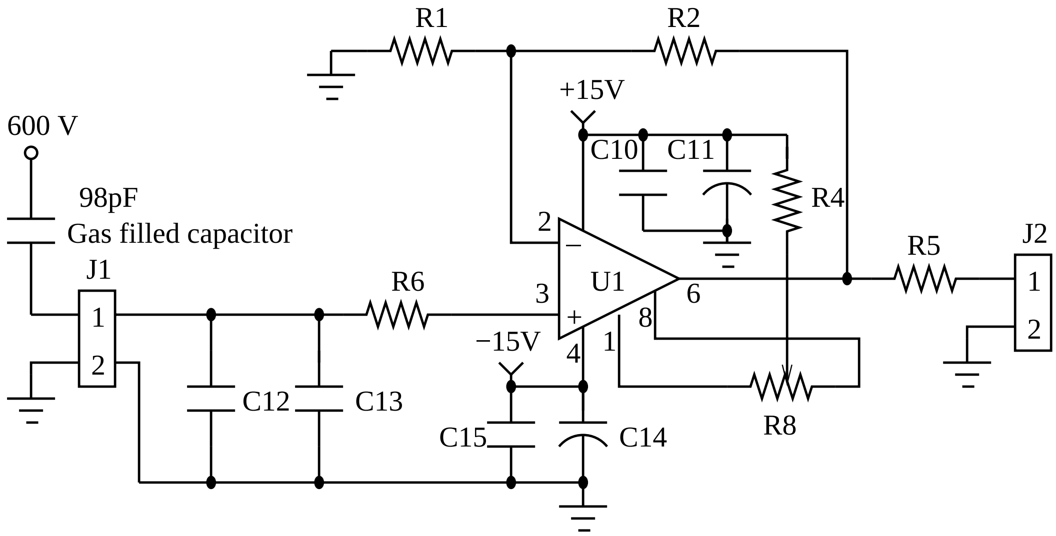

R1=680Ω R2=9.1k Ω R4=390Ω R5=75 Ω R6=470Ω R8=1k Ω

C10=0.1μF C11=2.2μF C12=0.1μF C13=0.1μF C14=2.2μF C15=0.1μF

U1: AD845

Fig. 3.5 Circuit diagram of voltage front end of the high voltage test setup.

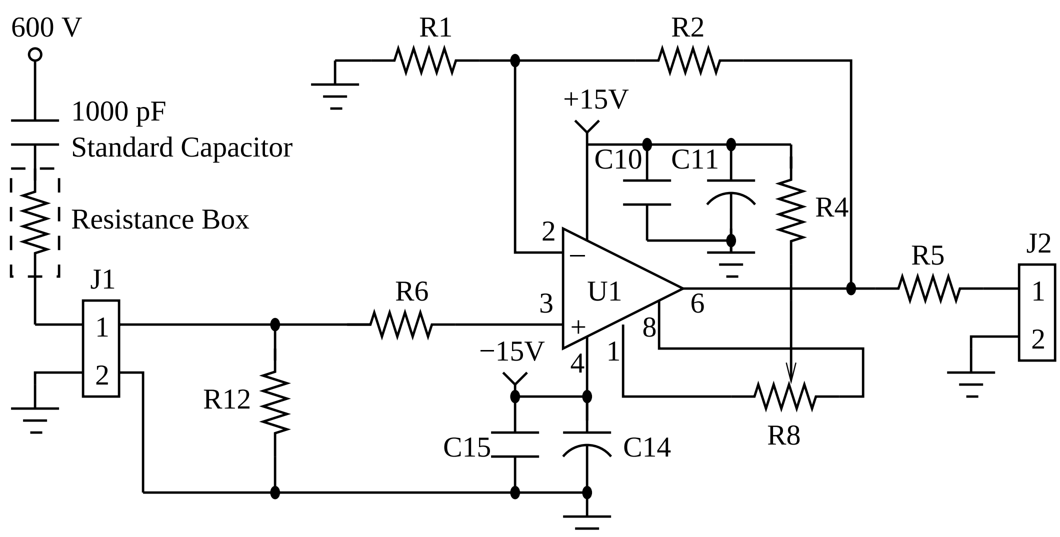

R1=200Ω R2=9.1k Ω R4=390Ω R5=75 Ω R6=470Ω R8=1k Ω

R12=470Ω C10=0.1μF C11=2.2μF C14=2.2μF C15=0.1μF U1:AD845

Fig. 3.6 Circuit diagram of current front end of the high voltage test setup.

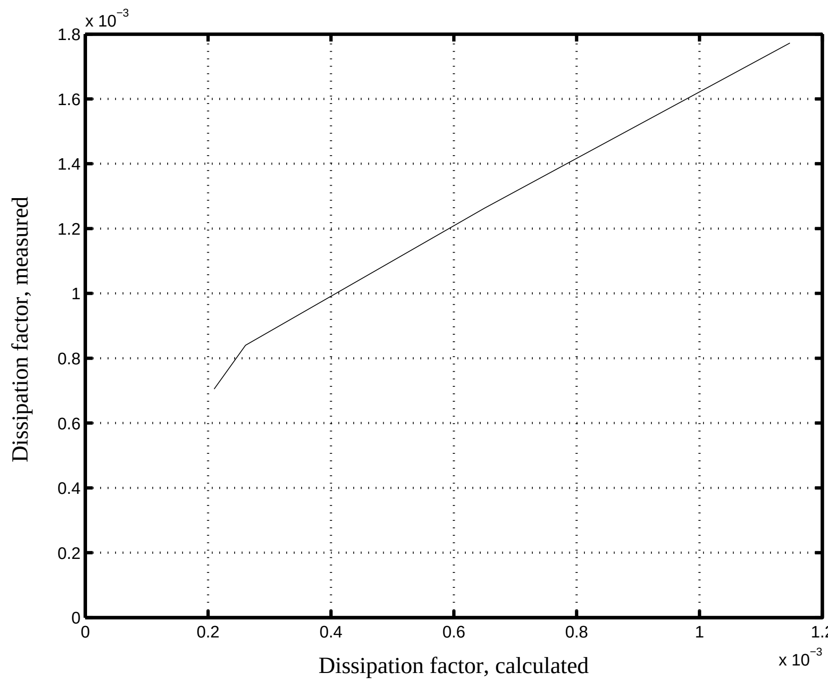

Fig. 3.7 Plot of dissipation factor measured values vs. calculated values for the circuit shown in Fig. 3.5 and Fig. 3.6.

3.4 Discussion

With the experimental setups involving DSO, the basic measurement scheme could be demonstrated. However, it was not possible to have good resolution in the measurement, as the number of bits were limited to 8 and record length limits the effectiveness of low pass filter. For $L = 8$, $\gamma = 10^{-4}$, the theoretical estimate of standard deviation of error as given in Table 2.1 is 64×10^{-6}. Hence, for better measurement resolution, we need to have higher L and γ, i.e. larger sampling rate/power line frequency ratio and larger record length. A low cost setup for this purpose is presented in the next chapter.

Chapter 4
Implementation with low sampling rate

This chapter aims at verifying the technique proposed in Chapter 2 by sampling the two signals at a rate lower than the power line frequency. First the numerical simulations were carried out. This was followed with the development of hardware setup for signal acquisition.

The two waveforms being processed for online measurement of dissipation factor are periodic and when sampled at a low rate will result in aliased periodic sequences which retain the same phase relationship as the original waveform and thus can be used for obtaining the $\tan\delta$ values.

Let the sampled voltage and current signals from the capacitor with dielectric under test be given as

$$s_1(n) = V_m \cos(2\pi n\, f_o / f_s) \tag{4.1}$$

$$s_2(n) = I_m \cos(2\pi n\, f_o / f_s + 0.5\pi - \delta) \tag{4.2}$$

By setting the sampling rate

$$f_s = f_o - f_x \tag{4.3}$$

we get the aliased waveforms as,

$$x_1(n) = V_m \cos(2\pi n\, f_x / f_s) \tag{4.4}$$

$$x_2(n) = I_m \cos(2\pi n\, f_x / f_s + 0.5\pi - \delta) \tag{4.5}$$

We see that the two waveforms x_1 and x_2 are periodic with frequency $f_x = f_o - f_s$, and retain the same phase relationship as s_1 and s_2.

The real advantage of the method is that the low sampling rate means a low data transfer rate and hence entire hardware can become inexpensive. Further the signal acquisition units can be put in a distributed manner for online monitoring of the dissipation factor at several places, all communicating the results to a central unit over a serial link (e.g. RS-232/ RS-485).

For better precision we need a higher order filtering, hence larger record lengths. Thus one can have a trade off between the low sampling rate for inexpensive instrumentation and the rate at which measurements are made. This generally should not be a problem because the dissipation factor varies slowly under normal aging process.

4.1 Numerical simulation

For simulation, we have taken V_m = 1, I_m =1, signal frequency f_o = 50 Hz, and sampling rate f_s = 45 sa/s. This results in aliased sinusoidal signals with frequency of 5 Hz. The signals retain the same phase relationship as the original signals. The simulations are carried out with 16 and 12 bit quantization for loss angle δ in the range of 0.005 – 0.05 radian range.

First the numerical simulation was carried out using a 9 k-tap FIR (designed using rectangular window low pass filter). The cut-off frequency of this filter is 0.005 Hz, i.e. $\gamma = 1.11\times10^{-4}$. Processing was done for sequence length of 50 k. The response becomes stable after 9 k samples. The average was taken over the remaining 41 k samples. The standard deviation is of the order of 0.3×10^{-6}, as expected.

For studying the effect of change in power line frequency, numerical simulation was carried out for different values of signal frequency f_o, in the 49–51 Hz range, keeping the sampling rate at f_s = 45 sa/s. This resulted in a aliased frequency over the range of 4–6 Hz. The result of simulation for f = 49.001 Hz are given in Table 4.1. As in the case of simulation for high sampling rate, here also the standard deviation depends on frequency. Error is low when the filter cut-off frequency is a sub-multiple of the second harmonic and it coincides with low pass filter notch.

In order to keep the errors low over the frequency range, we need a filter without ripples in the stop band. Hence simulations were carried out using 4th order Butterworth filter, with f_o varied over of 49-51 Hz. The filtering is done with cut-off frequency f_c = 0.005 Hz i.e. $\gamma = 1.11\times10^{-4}$. Processing was done for record length of 50 k samples. As the response stabilized after about 22500 samples, the statistical average was taken over the remaining 27,500 samples. Standard deviation was found to be independent of f_o variation. The results with f_o = 49.001 Hz and f_s = 45 Hz are presented in Table 4.2. We see that for δ = 0–0.05, $\sigma < 0.4\times10^{-6}$. Hence we conclude that IIR filter is a better option for low pass filter and by having a fourth order low pass filter we are able to use same filter over 49–51 Hz.

Table 4.1 Results of numerical simulation F: f = 49.001 Hz, f_s = 45 sa/s, L=16 bits. LPF: 9000-tap FIR filter (rectangular window) with $f_c \approx 0.005$ Hz or $\gamma = 1.11\times10^{-4}$.

δ (radians)	s_9 mean	s_9 max	s_9 min	σ
0	1.37670e-08	1.99506e-04	-1.99489e-04	1.40960e-04
0.005	4.99919e-03	5.19877e-03	4.79964e-03	1.40960e-04
0.006	6.00359e-03	6.20329e-03	5.80384e-03	1.40960e-04
0.007	7.00179e-03	7.20131e-03	6.80223e-03	1.40960e-04
0.008	8.00264e-03	8.20223e-03	7.80293e-03	1.40960e-04
0.009	9.00006e-03	9.19971e-03	8.80041e-03	1.40960e-04
0.01	9.99891e-03	1.01985e-02	9.79928e-03	1.40960e-04
0.02	1.99943e-02	2.01940e-02	1.97948e-02	1.40960e-04
0.03	2.99865e-02	3.01862e-02	2.97868e-02	1.40960e-04
0.04	3.99908e-02	4.01905e-02	3.97911e-02	1.40960e-04
0.05	4.99846e-02	5.01842e-02	4.97850e-02	1.40960e-04

Table 4.2 Results of numerical simulation G: f_o = 49.001 Hz, f_s = 45 sa/s, L =16 bits. LPF: fourth order Butterworth with $f_c \approx 0.005$ Hz or $\gamma = 1.11\times10^{-4}$.

δ (radians)	s_9 mean	s_9 max	s_9 min	σ
0	-3.65876e-08	2.49224e-07	-8.73748e-07	2.85187e-07
0.005	4.99800e-03	4.99844e-03	4.99730e-03	2.66166e-07
0.006	5.99678e-03	5.99723e-03	5.99566e-03	4.15117e-07
0.007	6.99939e-03	6.99979e-03	6.99839e-03	3.57557e-07
0.008	7.99874e-03	7.99905e-03	7.99784e-03	3.23471e-07
0.009	8.99807e-03	8.99852e-03	8.99699e-03	3.88240e-07
0.01	9.99519e-03	9.99547e-03	9.99423e-03	3.16065e-07
0.02	1.99906e-02	1.99910e-02	1.99901e-02	2.23438e-07
0.03	2.99857e-02	2.99861e-02	2.99845e-02	3.93453e-07
0.04	3.99941e-02	3.99946e-02	3.99936e-02	2.66432e-07
0.05	4.99853e-02	4.99856e-02	4.99843e-02	3.36899e-07

Table 4.3 Results of numerical simulation H: f_o = 50 Hz, f_s = 45 Hz, L=12 bits. LPF: 4th order Butterworth with $f_c \approx 0.005$ Hz or $\gamma = 1.11\times10^{-4}$.

δ (radians)	s_9 mean	s_9 max	s_9 min	σ
0	7.22568e-06	1.66789e-04	-1.69347e-04	9.90461e-05
0.005	4.98374e-03	5.13410e-03	4.81885e-03	7.85126e-05
0.006	6.00370e-03	6.12633e-03	5.89277e-03	6.56185e-05
0.007	6.97770e-03	7.13084e-03	6.78412e-03	9.91280e-05
0.008	8.00058e-03	8.13498e-03	7.84306e-03	7.67032e-05
0.009	8.98631e-03	9.11411e-03	8.84855e-03	8.68609e-05
0.01	9.99272e-03	1.01714e-02	9.79999e-03	1.12247e-04
0.02	1.99862e-02	2.01888e-02	1.98109e-02	1.12579e-04
0.03	3.00016e-02	3.01523e-02	2.98893e-02	7.25554e-05
0.04	3.99954e-02	4.02592e-02	3.97861e-02	1.40128e-04
0.05	5.00119e-02	5.01624e-02	4.98434e-02	1.01337e-04

Table 4.3 gives simulation results with L = 12, f_o = 50 Hz, f_s = 45 sa/s, with the same filter as before, we see that $\sigma < 1.5 \times 10^{-5}$. Figure 4.1 shows the plot of dissipation factor measured versus calculated values of Table 4.3.

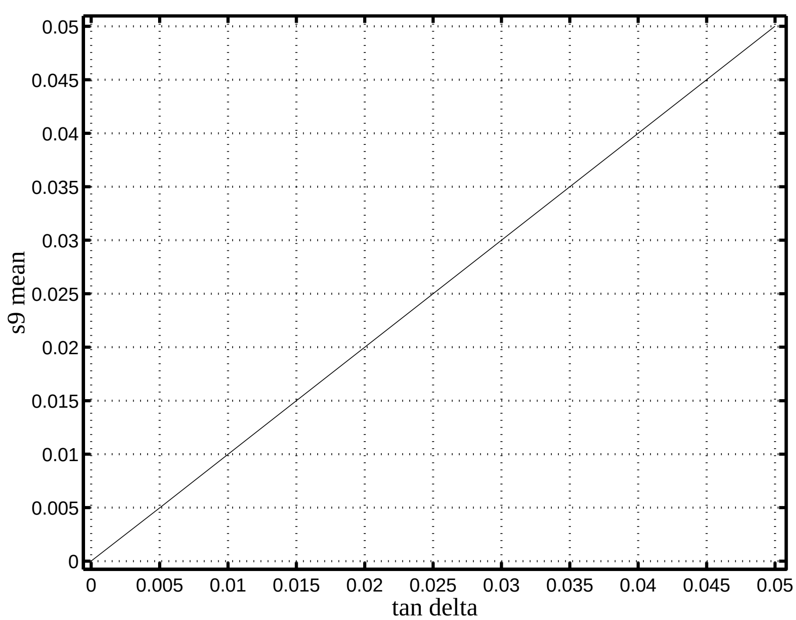

Fig. 4.1 Plot of dissipation factor measured vs. calculated values for results in Table 4.3

4.2 Hardware setup

Sampling at a low rate permits sample data transfer over serial interface, and this can be exploited for developing a low cost instrument. After considering various ADC chips and hardware configurations, the hardware circuit setup as given in Fig. 4.2 was designed. It has two 12-bit serial ADC's U1 and U2, ADS7822 [18].These are connected to a microcontroller U3, AT89C52 [19],[20]. The task of microcontroller is to acquire samples for the two ADC's serially and transfer those to the PC for processing using RS-232 link. The crystal connected to XTAL pins of U3 is of 11.0592 MHz for exact matching of the baud rates.

A stable reference voltage of 2.5 V is applied through U5 (3- terminal adjustable reference TL431, with cathode and reference pins shorted and a current limiting resistor of 470 Ω). The two signal inputs V_{in1} and V_{in2} are connected to the ADC's with a bypass capacitor of 0.1 μF for filtering. The clock and chip select of the two ADC's are shorted and connected to pin 2.4 and pin 2.7 of the microcontroller respectively. These pins act as a common chip select and clock to both the ADC's. The data_out pin of the two ADC's are given to the port pins 2.5 and 2.6. The microcontroller is given the external trigger i.e. sampling signal of 45 Hz square wave of 0-5V on port pin 3.3. The supply pins of all the ICs are bypassed with 0.1 μF capacitor.

The TXD and RXD pins of the microcontroller are connected to the T2in and R2out pins of the RS232 driver U4, MAX232. The pins T2out (pin 7) and R2in (pin 8) of the U4 are connected to the transmit and receive (pins 2 and 3) of the female DB9 connector. Pin number 5 is the ground of this connector. The entire circuit operates with a single 5 V supply. The input signal ranges are 0-2.5 V unipolar. The PCB layout was designed, and the board was fabricated and assembled.

An assembly language program was written into the microcontroller for reading the data from the 12-bit ADCs. The stack pointer is initialized to point to a location above the bit addressable area. The port pins 3.3, 2.6, 2.7, 2.4 are initialized. The timer 0 of microcontroller is set in mode 1 and the timer 1 is set in mode 2. The baud rate is set to 9600. The microcontroller is initialized for serial communication. After that serial and timer 0 interrupts are enabled. Pin 3.3 is polled for its high status, once it goes high the program goes to the read ADC routine. Here the data from the 2 ADCs are read into the

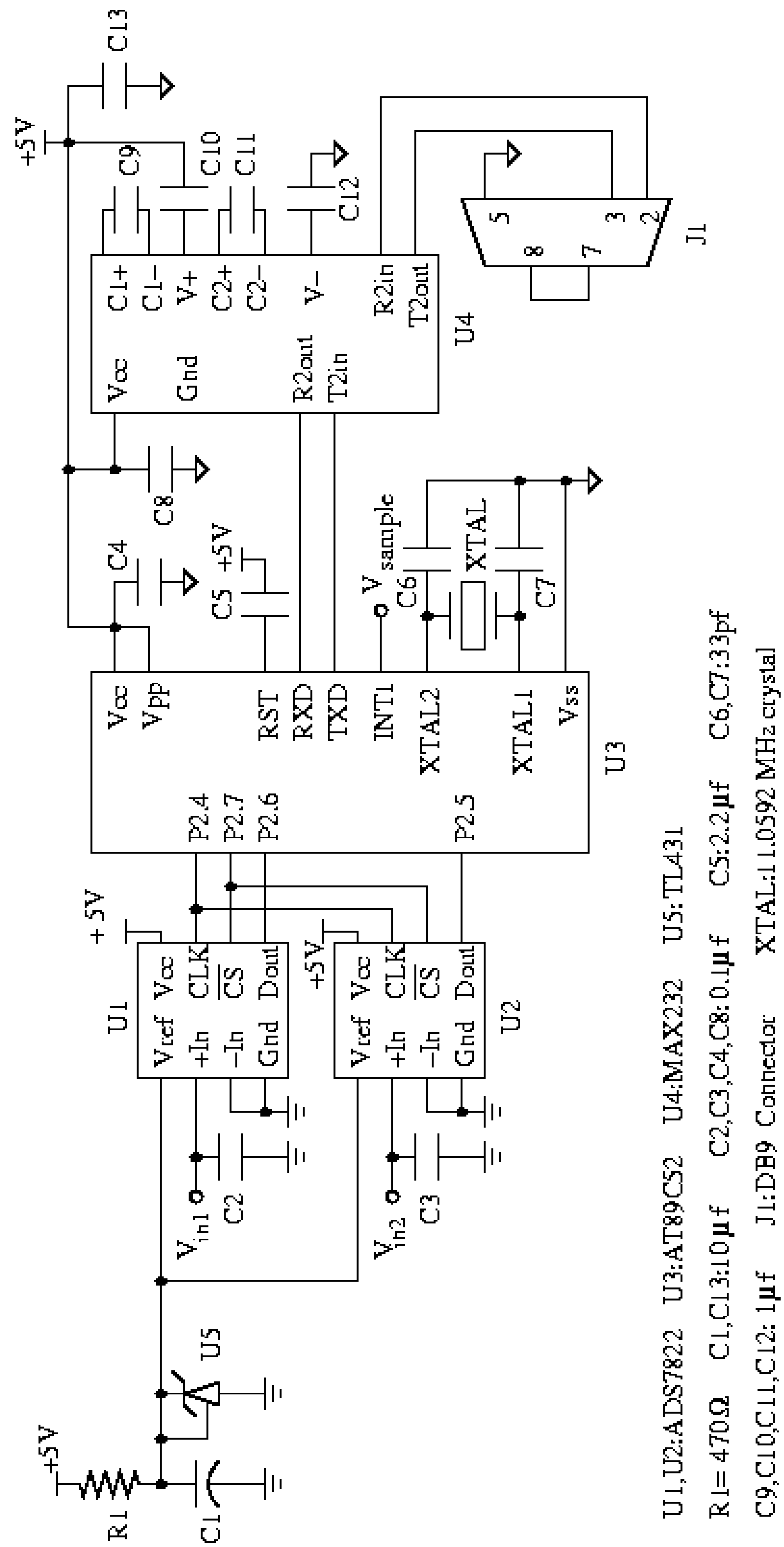

Fig. 4.2 Hardware circuit diagram for signal acquisition with $f_s < f_o$.

microcontroller’s bit-addressable registers, bit-by-bit alternately for the 2 channels. Also the 1’s complement of the data bytes are stored in the microcontroller bit-addressable registers. After reading the data, the first start byte is loaded into the serial buffer and then transmission starts. If the transmission is over, the ti_flag is set and then the second start byte is sent. The channel-1 higher byte is then sent, followed by the lower byte. The channel-2 bytes are sent next followed by 1’s complement of the 4 bytes.

The data pattern has two start bytes to start the communication process, followed by four data bytes of the two channels and then the 1’s complement of the data bytes as given below:

Start Bytes : <2A><3F>

4 data bytes : <Ch1MSB><Ch1LSB><Ch2MSB><Ch2LSB>

4 complement bytes : <Ch1’MSB><Ch1’LSB><Ch2’MSB><Ch2’LSB>

The complement of the data bytes are sent to detect transmission errors. In case of a sample being incorrectly received, the previous sample values is retained.

Data reception is handled on the PC through program “SERIAL.C” written in C. It waits for the start bytes. The next 8 bytes are taken as the data bytes The file is processed to get the dissipation factor value.

4.3 Experimentation results

The circuit setup is shown in Fig. 4.3. The test capacitor is obtained by connecting capacitance C_x with a series resistance R_x to get a range of tanδ values.

$$\tan\delta = \omega C_x R_x \tag{4.6}$$

This current is then sensed by giving to an I-V converter built using U1b from quad op-amp TL084, selected for low input bias current and offset current and high input impedance.

The test capacitor was excited by a sinusoidal output from a signal generator (HP 33120A) with a offset of 1.25V and a peak-to-peak voltage of 2.4V. The voltage signal is given through a non-inverting buffer to the input of the second ADC. The signal corresponding to the current is obtained in terms of a voltage signal from the I/V converter circuit. A reference of 1.25 V is given to the non-inverting input of the op-amp U1B since the dc shift from the supply gets blocked because of the series capacitor. The output data of the op-amps is given to the input of the two ADCs shown in Fig. 4.2. The signal acquisition is done at 45 sa/s. by providing a 45 Hz 0-5 V square wave (from HP 33210A) to the microcontroller trigger pin INT1.

The sampled values were acquired through PC serial port and stored as files of 61 k samples. Several methods for processing were used to study their relative merits. Band pass filtering was done at the input to remove dc offsets and noise. Two types of filtering were done: wide-band and narrow-band. Cascading of the band pass filters was also used. For low pass filtering, first a FIR filter designed with rectangular window of order 15 k was used. Later a Butterworth filter of fourth order was used. Next cascade of Butterworth and FIR filter was used. Inverse Chebyshev filter of third order was also used. The results for these filters are given here.

For excitation frequency f_o = 50 Hz and sampling frequency f_s = 45 sa/s, the acquired waveforms are equivalent to 5 Hz waveform sampled at 45 Hz. In the first processing, the inputs from both channels were band pass filtered. The band pass filter filter used was a FIR filter of order 1000 (designed using a Hamming window) with a pass band of 3-7 Hz. The low pass filter used was a fourth order Butterworth filter, with cut-off frequency f_c = 0.005 Hz, i.e. $\gamma = 1.11\times10^{-4}$. The low pass filter output stabilizes

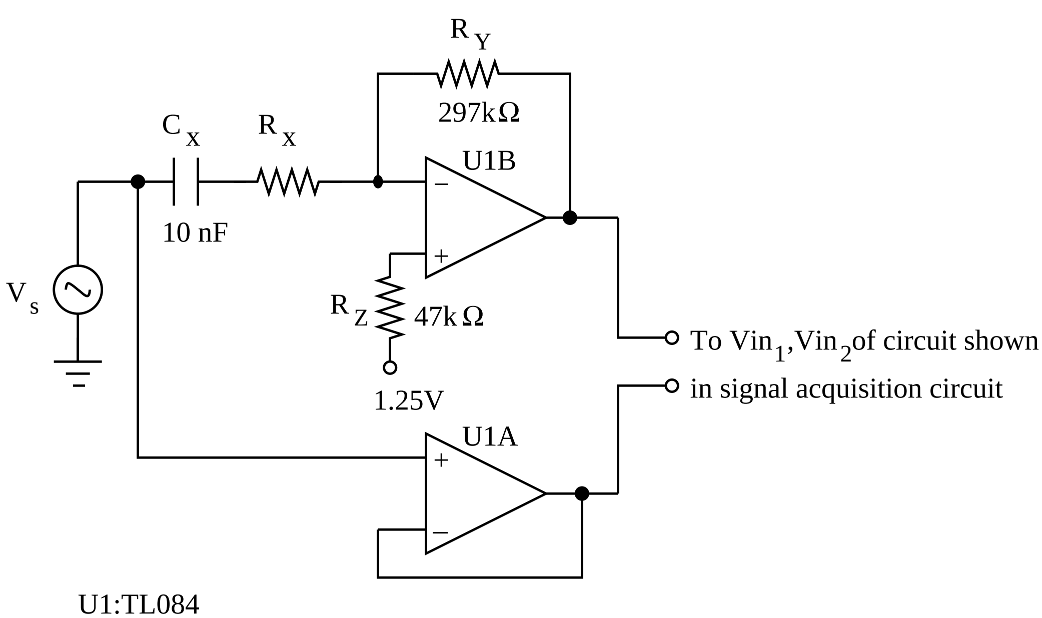

Fig. 4.3 Test setup using an I/V converter.

after about 46 k samples. Over the last 15 k samples the average was taken. The results are shown in Table 4.4. The standard deviation is of the order of 10^{-3}.

Next the fourth order Butterworth low pass filter and FIR low pass filter of order 15 k were cascaded. The inputs were band pass filtered as earlier. The LPF response became stable after 56 k samples. The average was taken over the last 5 k samples. The results are shown in Table 4.5. The standard deviation was found to be in the range of 4×10^{-4}, which was still higher than the acceptable standard deviation of 0.5×10^{-4}.

Next, the effect of narrowing the band pass filter was investigated. The 1000-tap FIR band pass filter (with Hamming window) with a pass band of approximately 0.4 Hz centered at the dominant frequency component was used for input filtering. The dominant frequency component was calculated using the power density spectrum of the input waveforms. The low pass filtering in the processing was done using 4th order Butterworth with cut-off frequency of 0.005 Hz cascaded with 15 k tap low pass FIR. The averaging was done over the last 5 k samples of record length of 61 k samples. The results are shown in Table 4.6. In some cases, the standard deviation is reduced but is still above the acceptable values.

Table 4.4 Experimental setup results with BPF of 3-7 Hz , Butterworth LPF of 4th order with $\gamma = 1.11\times10^{-4}$.

R_s(kΩ)	tanδ	s_9 mean	s_9 max	s_9 min	σ
1.19	3.95e-03	3.62e-03	8.03e-03	1.25e-03	2.46e-03
2.71	8.94e-03	2.87e-03	5.58e-03	5.06e-04	1.80e-03
3.86	1.27e-02	1.40e-02	1.61e-02	1.26e-02	1.01e-03
4.62	1.52e-02	1.18e-02	1.67e-02	6.41e-03	3.20e-03
5.53	1.82e-02	1.96e-02	2.59e-02	1.42e-03	4.41e-03
7.10	2.34e-02	2.30e-02	2.51e-02	2.09e-02	1.49e-03
8.29	2.73e-02	2.61e-02	2.81e-02	2.32e-02	1.49e-03
9.83	3.24e-02	2.88e-02	3.19e-02	2.40e-02	2.79e-03
11.78	3.88e-02	3.76e-02	4.17e-02	3.21e-02	3.04e-03
14.91	4.92e-02	5.07e-02	5.30e-02	4.69e-02	1.93e-03

Table 4.5 Experimental setup results with BPF of 3-7 Hz and Butterworth LPF of 4th order and cascaded with FIR LPF of order 15 k, with effective f_c = 0.003 Hz or γ = 6.66×10^{-5}.

R_s(kΩ)	tanδ	s_9 mean	s_9 max	s_9 min	σ
1.19	3.95e-03	3.21e-03	3.64e-03	2.56e-03	2.98e-04
2.71	8.94e-03	2.48e-03	3.04e-03	2.19e-03	2.75e-04
3.86	1.27e-02	1.38e-02	1.40e-02	1.34e-02	2.18e-04
4.62	1.52e-02	1.27e-02	1.32e-02	1.17e-02	4.78e-04
5.53	1.82e-02	1.96e-02	1.97e-02	1.93e-02	9.32e-05
7.10	2.34e-02	2.31e-02	2.33e-02	2.30e-02	1.12e-04
8.29	2.73e-02	2.58e-02	2.60e-02	2.55e-02	1.36e-04
9.83	3.24e-02	2.90e-02	2.91e-02	2.87e-02	1.00e-04
11.78	3.88e-02	3.76e-02	3.81e-02	3.73e-02	2.59e-04
14.91	4.92e-02	5.02e-02	5.06e-02	4.96e-02	3.39e-04

Table 4.6 Experimental setup results using BPF with pass band 0.4 Hz, Butterworth LPF of 4th order cascaded with 15 k-tap FIR.

R_s(kΩ)	tanδ	s_9 mean	s_9 max	s_9 min	σ
1.19	3.95e-03	1.27e-03	1.93e-03	9.66e-04	2.37e-04
2.71	8.94e-03	2.15e-03	2.57e-03	1.98e-03	1.59e-04
3.86	1.27e-02	1.45e-02	1.46e-02	1.43e-02	6.95e-05
4.62	1.52e-02	1.50e-02	1.53e-02	1.38e-02	4.05e-04
5.53	1.82e-02	1.92e-02	1.95e-02	1.88e-02	1.77e-04
7.10	2.34e-02	2..43e-02	2.43e-02	2.43e-02	1.72e-05
8.29	2.73e-02	2.45e-02	2.49e-02	2.35e-02	3.97e-04
9.83	3.24e-02	2.88e-02	2.90e-02	2.83e-02	1.80e-04
11.78	3.88e-02	3.87e-02	3.89e-02	3.81e-02	2.65e-04
14.91	4.92e-02	4.72e-02	4.87e-02	4.59e-02	9.09e-04

In order to further reduce the standard deviation, the inverse Chebyshev filter of third order was implemented with a cut-off frequency of 0.002 Hz and 80 dB attenuation in the stop band. Band pass filtering of the input was done using 1000-tap FIR (designed using Hamming window) with pass band of 3-7 Hz. The response becomes stable after 46 k samples. Hence the average was taken over the last 15 k samples. The results are shown in Table 4.7.The standard deviation is mostly in the expected range of 10^{-5}.

To improve the results further, the input band pass filter width was narrowed to a range of 0.4 Hz centered at dominant signal frequency component. The low pass filter was the same, inverse Chebyshev filter of order 3 and 80 dB attenuation in stop band and cut-off frequency of 0.002 Hz i.e. $\gamma = 4.44\times10^{-5}$. The output stabilized after 46 k samples. The averaging was done over the last 15 k samples. The results are shown in Table 4.8. We see that the standard deviation is further reduced in most of the cases.

Table 4.7 Experimental setup results using BPF of 3-7 Hz, Chebyshev LPF of 3rd order with $\gamma = 4.44\times10^{-5}$.

R_s(kΩ)	tanδ	s_9 mean	s_9 max	s_9 min	σ
1.19	3.95e-03	5.56e-03	5.96e-03	5.21e-03	2.14e-04
2.71	8.94e-03	5.81e-03	5.88e-03	5.68e-03	5.91e-05
3.86	1.27e-02	1.31e-02	1.32e-02	1.29e-02	8.31e-05
4.62	1.52e-02	1.60e-02	1.61e-02	1.60e-02	4.55e-05
5.53	1.82e-02	1.58e-02	1.60e-02	1.57e-02	9.53e-05
7.10	2.34e-02	2.27e-02	2.28e-02	2.27e-02	3.39e-05
8.29	2.73e-02	2.68e-02	2.70e-02	2.67e-02	9.97e-05
9.83	3.24e-02	2.76e-02	2.78e-02	2.74e-02	9.28e-05
11.78	3.88e-02	3.89e-02	3.90e-02	3.88e-02	6.53e-05
14.91	4.92e-02	4.79e-02	4.81e-02	4.77e-02	1.10e-04

It is seen that, in some cases, narrowing the band pass filter has helped in reducing the standard deviation. Next, a cascade of two band pass filters was implemented, with the rest of the processing remaining the same. These results are shown in Table 4.9. It is found that standard deviation is slightly improved, as compared to the results given in Table 4.8. The standard deviation in most of the cases is below 7×10^{-5}, which is close to the acceptable standard deviation of 5×10^{-5}. Best fit line, using GNUPLOT, has slope of 0.981239 and offset of 2.38095×10^{-4}.

Table 4.8 Experimental setup results using BPF with pass band 0.4 Hz, Inverse Chebyshev LPF of 3rd order with $\gamma = 4.44\times10^{-5}$.

R_s(kΩ)	tanδ	s_9 mean	s_9 max	s_9 min	σ
1.19	3.95e-03	6.76e-03	7.55e-03	6.05e-03	4.31e-04
2.71	8.94e-03	7.84e-03	7.87e-03	7.73e-03	3.69e-05
3.86	1.27e-02	1.32e-02	1.37e-02	1.36e-02	2.74e-05
4.62	1.52e-02	1.67e-02	1.68e-02	1.67e-02	2.74e-05
5.53	1.82e-02	1.70e-02	1.72e-02	1.68e-02	1.12e-04
7.10	2.34e-02	2.31e-02	2.33e-02	2.30e-02	9.68e-05
8.29	2.73e-02	2.57e-02	2.58e-02	2.56e-02	7.72e-05
9.83	3.24e-02	2.85e-02	2.86e-02	2.85e-02	2.82e-05
11.78	3.88e-02	3.97e-02	3.95e-02	3.98e-02	9.01e-05
14.91	4.92e-02	4.80e-02	4.81e-02	4.79e-02	6.86e-05

4.4 Discussion

Numerical simulation results verified that the aliased periodic waveforms, obtained by using $f_s < f_o$ can be processed to get the tanδ. Fourth order Butterworth filter with $\gamma = 1.11\times10^{-4}$ gave standard deviation comparable to the theoretical estimates of RMS value of error for L = 12 and 16. Also it is seen that with this filter, standard deviation does not depend on small variation in f_o. Low pass filter of inverse Chebyshev type further reduces the standard deviation.

A hardware for signal acquisition with serial data transfer using RS-232 at 9600 baud was developed. It consists of two 12-bit ADC chips interfaced through synchronous serial interface to a microcontroller and RS-232 driver. The input waveforms have to be

Table 4.9 Experimental setup results using cascade of two BPF with pass band 0.4 Hz, Inverse Chebyshev LPF of 3rd order with $\gamma = 4.44\times10^{-5}$.

R_s(kΩ)	tanδ	s_9 mean	s_9 max	s_9 min	σ
1.19	3.95e-03	6.75e-03	7.55e-03	6.03e-03	4.20e-04
2.71	8.94e-03	7.91e-03	7.94e-03	7.80e-03	3.61e-05
3.86	1.27e-02	1.37e-02	1.38e-02	1.37e-02	2.56e-05
4.62	1.52e-02	1.67e-02	1.68e-02	1.67e-02	2.42e-05
5.53	1.82e-02	1.71e-02	1.72e-02	1.68e-02	1.00e-04
7.10	2.34e-02	2.31e-02	2.32e-02	2.29e-02	9.18e-05
8.29	2.73e-02	2.58e-02	2.59e-02	2.57e-02	7.10e-05
9.83	3.24e-02	2.86e-02	2.87e-02	2.86e-02	3.41e-05
11.78	3.88e-02	3.98e-02	3.96e-02	3.96e-02	8.66e-05
14.91	4.92e-02	4.79e-02	4.80e-02	4.78e-02	6.38e-05

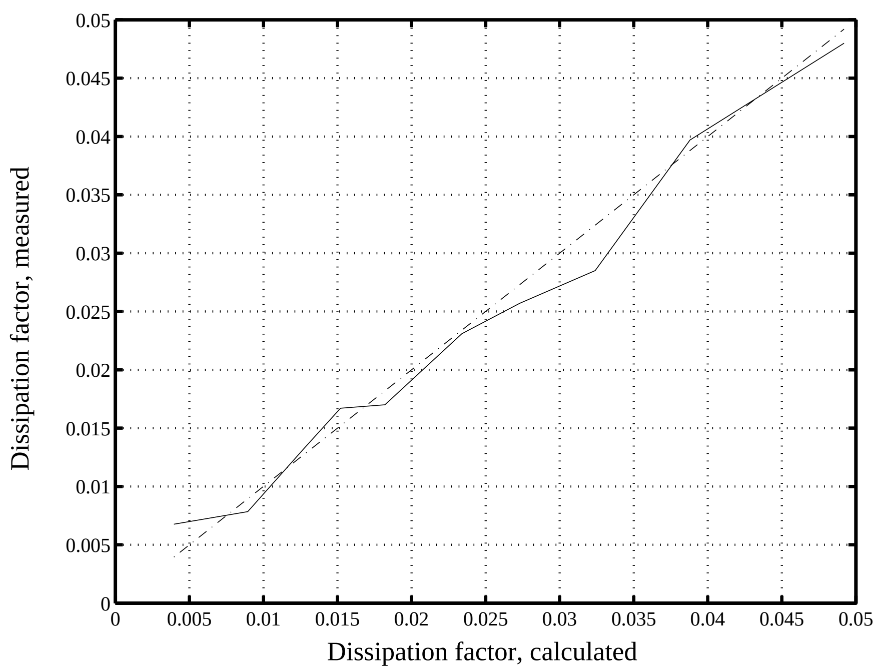

Fig. 4.4 Plot of dissipation factor measured values vs. calculated values for circuit shown in Fig. 4.3.

scaled and shifted in 0-2.5 V input unipolar range. Simultaneous sampling of the two input channels is done in response to external pulses. Experimental setup used 30 V_{pp} excitation with f_o = 45 sa/s. It was found that the low pass filtering with Butterworth filter was not adequate. Pre-processing of the inputs with narrow band pass filter was to reduce the noise introduced in the signal acquisition and distortions due to transmission errors. Standard deviation $\approx 5 \times 10^{-5}$, could be obtained by using 3rd order inverse Chebyshev filter with $\gamma = 4.44 \times 10^{-5}$. Because of the bandpass filter and low pass filter, the system has a response time of about 46 k samples. i.e. $\approx$ 16 minutes.

Chapter 5

Summary and conclusions

Periodic online measurement of dielectric dissipation factor can be used for monitoring the condition of insulation in high voltage equipment in order to ensure their safe and reliable operation. This project involved investigating, through numerical simulation and experimental set-up, a technique based on digital processing of voltage and current signals. The technique measures the dissipation factor by dividing the low-pass filtered product of voltage and current signals by the RMS values of the two signals (obtained as the square root of the low-pass filtered square of the two waveforms). The measurement update rate depends on the response time of the low pass filters.

The application is for developing instruments for online monitoring of realistic range of dissipation factor of bushing insulation in power transformers in the 5-50 $\times 10^{-3}$ range, with a resolution better than 5×10^{-5}. Pandey [14] has earlier carried out a theoretical analysis for estimating the measurement error, as a function of number of quantization bits L and the normalized cutoff frequency γ (= f_c / f_s). It was assumed that no errors were introduced due to finite precision arithmetic in processing. The analysis, presented in Chapter 2, showed that the ac RMS value of the error is given as $\sigma = 2^{-L}\sqrt{8\gamma/3}$. Thus for $\sigma = 5 \times 10^{-5}$, we need $\gamma = 6.14 \times 10^{-5}$ and 1.57×10^{-2} for $L = 8$ and 12 respectively. As long as the filter eliminates the second harmonic component in the products, the exact value of power line frequency is not critical for this method. Since the error depends on normalized cutoff frequency, it is possible to have a trade-off between measurement update rate and the sampling rate.

Two types of implementations of the technique were investigated. In the first implementation, for power line frequency $\approx$ 50 Hz, simultaneous sampling of the two signals is carried out at 50 k sa/s. Numerical simulations verified the theoretical analysis results. Further, the use of FIR filters was found to give large errors, when the power line drifted from 50 Hz, because of imperfect canceling of the second harmonic due to ripples in the filter stop band. It was established that 4th order Butterworth filter could be used effectively. Experimental investigation with this sampling rate was carried out by using a

2-channel DSO for signal acquisition, on a 30 V_{pp} set-up with an R-C circuit simulating the lossy dielectric and using an I/V converter circuit for current sensing. Subsequently a 600 V set-up with a resistive shunt for current sensing was used. In both the cases, recorded sequences were transferred to a PC by using serial interface, and the data were processed offline, using Matlab and floating point arithmetic, with different processing parameters. The precision obtainable was in accordance with numerical simulation results. It was limited by 8-bit quantization available in the DSO. Also the relatively small sequence record length restricted the use of low filter cutoff frequency.

Next, we investigated a novel technique for developing a low cost signal acquisition and processing system. In this technique, the two signals are sampled at a rate lower than power line frequency, resulting in aliased low frequency periodic waveforms which retain the phase relationship of the original waveforms. Thus, we can carry out signal acquisition and online processing or data transfer at a low rate, and still get the desired precision. Since the digital filters are operating at low rate, measurement update rate will correspondingly decrease. Numerical simulations, with power line frequency ≈ 50 Hz and simultaneous sampling of the two signals at 45 sa/s showed that the technique can be used for getting the desired results. For experimental set-up, a low cost signal acquisition board with a two 12-bit ADC chips with synchronous serial interface and a micro-controller was developed. The sampling is done simultaneously on the two inputs with 0-2.5 V range, triggered by external 0-5 V pulses. The sample bytes are transferred online from the micro-controller over RS-232 link to a PC for processing. Experimental set-up was tested on a 30 V_{pp} set-up. It was observed that there were a small but significant number of transmission errors. Retaining the previous sample values in case of lost samples, and pre-processing the input sequences by a bandpass filter with normalized bandwidth of 0.008 centered at the aliased power-line frequency could obtain acceptable precision.

The investigations have indicated that floating point processing is essential for obtaining the desired precision. Further, simultaneous sampling of the signals is required in order to eliminate offset corrections for drift in power line frequency.

Based on our investigations with the first implementation, an instrument for measurements at high update rate can be developed by using a floating point DSP processor based board with two channel 12-bit simultaneous sampling of the signals at 50 k sa/s or higher. After processing, measurement results can be transferred with a serial link. Based on investigations with the second technique, a low cost instrument can be developed using a sampling rate lower than the power line frequency. In this system, the signal acquisition front-end will sample the signals and transmit these serially for processing by a central unit. This system will have a low measurement update rate. This may be appropriate for online condition monitoring of transformer bushings, but may not be suitable for applications requiring high speed measurement.

Appendix A Filter Testing

Low pass filter

The filters are tested for their magnitude response by applying an impulse as the input and then computing the magnitude spectrum of the output, which is then converted to dB scale. The response of FIR low pass filter using rectangular window is shown in Fig. A.1. The response of Butterworth low pass filter of fourth order with cut-off frequency of 0.005Hz is shown in Fig. A.2.

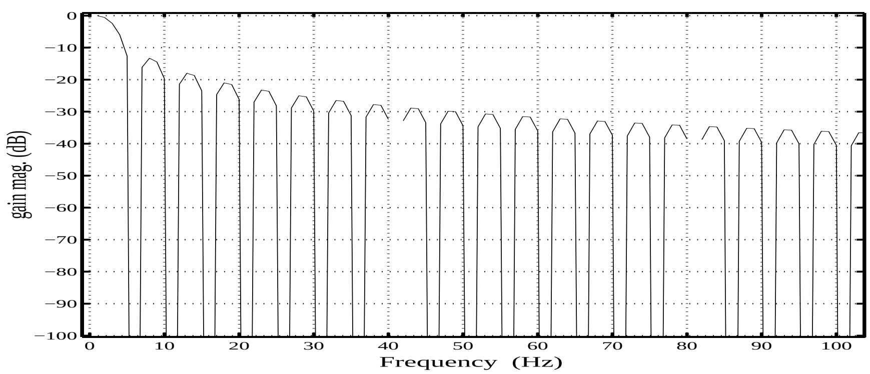

Fig. A.1 Response of 10 k order FIR filter used in simulation A, f_o = 50 Hz, f_s = 50 k sa/s, $f_c \approx$ 5 Hz.

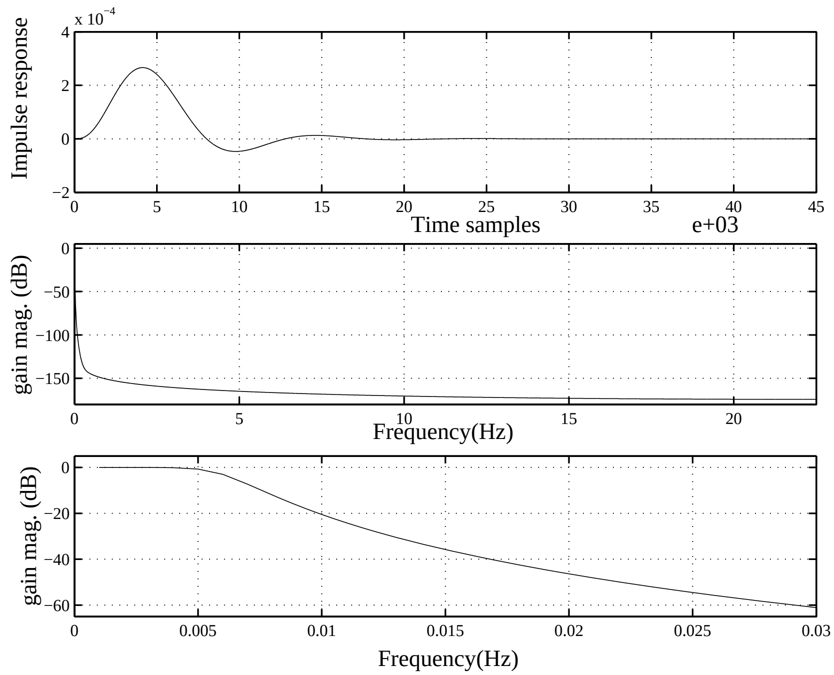

Fig. A.2 Response of 4th order Butterworth low pass filter with f_c = 0.005 Hz, f_s = 45 sa/s. The lower of two magnitude response shows a zoomed response in low frequency range.

Band pass filter

The same technique as that used for low pass filter testing was used to check the band pass filter response. The response of the narrow bandpass filter is given in Fig. A.3. In order to check the linearity of the implementation signal with frequencies lying in the pass band range of filter with different amplitudes were applied and the output was found to be of the expected amplitude.

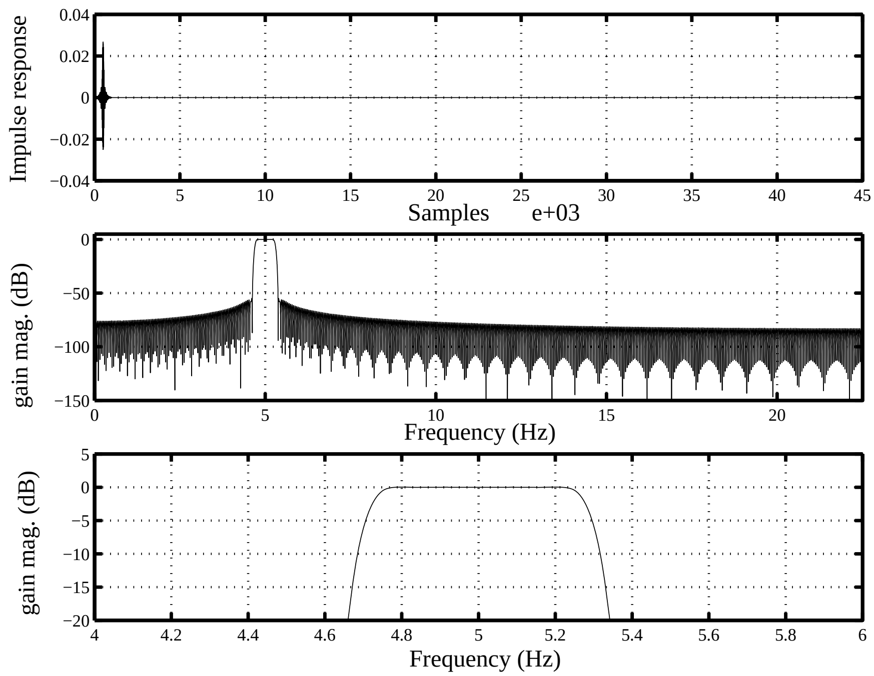

Fig. A.3 Response of FIR band pass filter (designed using Hamming window). The lower of the two magnitude response shows the zoomed response about the center frequency.

Appendix B Hardware testing and PCB layouts

The baud rate was checked by continuously sending the byte “55H” from the microcontroller via RS-232 driver to the PC serial port. The Tx signal was observed on the CRO. The rate was found to be 9618 bps. Then the same byte was continuously transmitted from PC via the serial port and the Rx signal was observed on CRO. The rate was found to be 9616 bps. Thus the two rates match.

To measure transmission error, between the PC and the microcontroller, data bytes are loaded in microcontroller and transmitted serially to the RS-232 driver and then received in the PC. The data recorded on the PC showed transmission errors of about 1%. It was decided to send the data bytes and its 1’s complement. This was done for counts loaded over the range of 0000 to 0FFF in the microcontroller. The bytes for which the data and its complement do not match are rejected at the receiver side. When a sample value is found corrupted, it is replaced with the previous sample.

The hardware was tested by applying dc signal to the input of the two ADCs, and the standard deviation was calculated. The results are given in the Table B.1. It is found that the standard deviation is less than 1. Then a common signal is applied to the both the inputs. Dissipation factor was calculated to be 0.999671 which is very close to 1.

Table B.1 Results with dc signal given to the circuit shown in Fig. 4.1.

Applied Voltage	**Expected Integer**	**Channel 1 mean**	**Channel 2 mean**	σ_{Ch1}	σ_{Ch2}
0 V	0	0	0	0	0
0.506 V	829	832.4	832.5	0.52	0.52
1.001 V	1638	1644.7	1644.9	0.80	0.75
1.50 V	2466	2472.7	2472.6	1.04	1.05
2.00 V	3283	3294.8	3294.7	0.86	0.86
2.50 V	4095	4095	4095	0	0

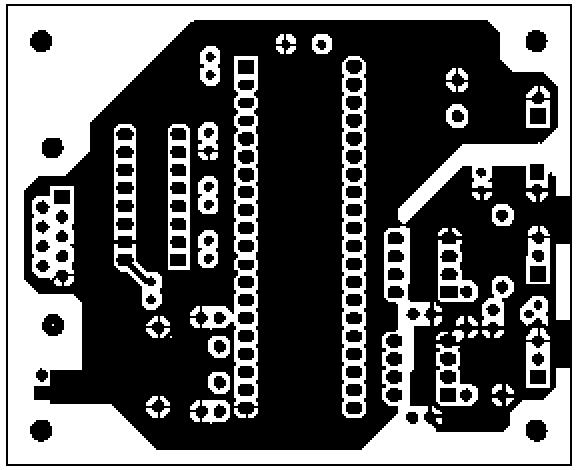

Solder Side of the PCB

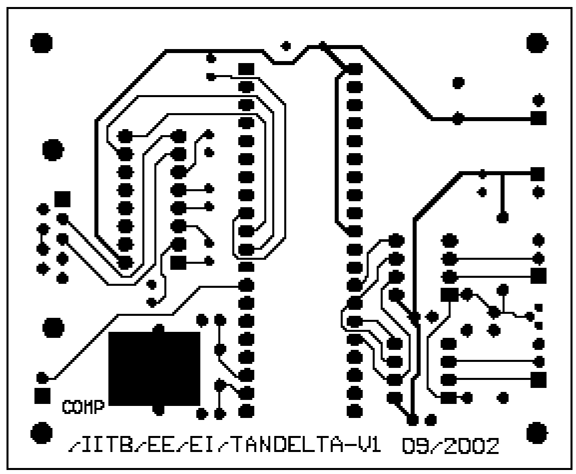

Component Side of the PCB

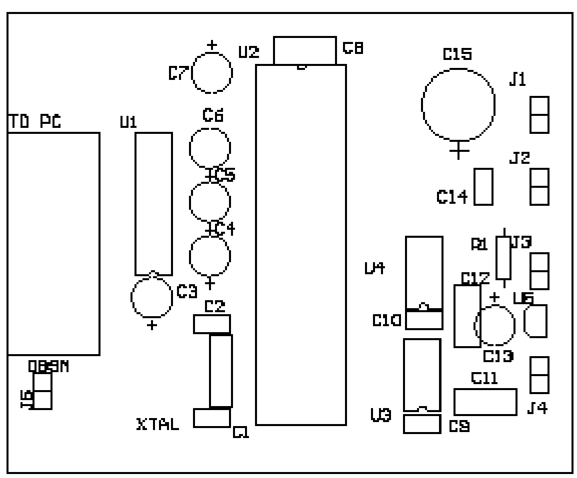

Top view of the PCB

Fig. B.1 PCB Layout

References

1. D. Kind, *An Introduction to High Voltage Experimental Technique*, New Delhi: Wiley Eastern, 1978.
2. E. Kuffel, and M. Abdullah, *High Voltage Engineering*, Oxford: Pergamon, 1970.
3. D.V. Razevig, *High Voltage Engineering*, Delhi: Khanna, 1972.
4. E.W. Golding, *Electrical Measurements and Measuring Instruments*, 4th edition, London: Pitman, 1955.
5. P. Vujovic, R.K. Fricker, J.A. Ehrich, and A.R.Young , "Development of an on-line continuous tanδ monitoring system," *IEEE International Symposium on Electrical Insulation*, Pittsburgh, 1994, pp. 50-53.
6. R.K. Fricker, "Monitoring HV insulation online," *Transmission and Distribution World*, vol. 48, no. 4, 1996, pp. 26-37.
7. S.M. Mahmud, A. Rusek, and S. Ganesan, "A microprocessor based dual slope phase meter," *IEEE Trans. Instrumentation & Measurement*, Vol. 37, September 1988, pp. 374-278.
8. K.M. Ibrahim and M.A.H. Abdul Karim, "A novel digital phase meter," *IEEE Trans. Instrumentation and Measurement*, vol-IM-36, September 1987, pp. 711-716.
9. T.S. Rathore and L.S. Mombasawala, "An accurate digital phase measurement scheme," *Proc. IEEE*, vol. 72, March 1987, pp. 297-298.
10. D. Allan, M. Blundell, K. Boyd, and D. Hinde, "New techniques for monitoring the insulation quality of in-service HV apparatus," *IEEE Trans. Electrical Insulation*, vol. 27, no. 3, June 1992, pp. 578-585.
11. N.A.F. Jaeger, G.S. Polovick, H. Kato, and S.E. Cherukapalli, "Online dissipation factor monitoring of high voltage current transformers and bushings," *CIGRE*, Session 1998.
12. P. Wang, M.R. Raghuveer, W. McDermid, and J.C. Bromley, "A digital technique for the online measurement of dissipation factor and capacitance," *IEEE Trans. on Dielectrics and Electrical Insulation*, vol.8, no.2, April 2001, pp. 228-232.

13. B. Djokic, and E. So, “Phase measurement of distorted periodic signals based on nonsynchronous digital filtering,” *IEEE Trans. Instrumentation & Measurement*, vol. 50, no.4, August 2001, pp. 864-867.
14. P.C. Pandey, “Me*asurement of very low tanδ*,” personally communicated note, IIT Bombay, prepared March 1997, revised November 1997.
15. J.G. Proakis and D.G. Manolakis, *Digital Signal Processing*, 3rd edition, New Delhi: Prentice Hall, 1999.
16. A.V. Oppenheim and R.W. Schafer, *Digital Signal Processing*, 2nd edition, New Delhi: Prentice Hall, 1994.
17. S.K. Mitra, *Digital Signal Processing: a Computer-Based Approach*, New Delhi: Tata McGraw-Hill, 2001.
18. “ADS7822 Datasheet,” http://www-s.ti.com/sc/ds/ads7822.pdf, accessed in September 2002.
19. K.J. Ayala, *The 8051 Microcontroller Architecture: Programming & Appl-ications*, 2nd edition, Mumbai: Penram International, 1996.
20. Atmel Corp., *Microcontroller Data Book*, San Jose, California, 1997.